I&EC research
Industrial & Engineering Chemistry Research

pubs.acs.org/IECR
Article

Dynamic Scheduling: A Comparison of High-Fidelity Models with Local Optimization versus Surrogate Models with Global Optimization

Chrysanthi Papadimitriou, Michael Baldea, and Alexander Mitsos*

Cite This: *Ind. Eng. Chem. Res.* 2025, 64, 21641−21657
Read Online

ABSTRACT: Flexible process operation supports demand-side management under fluctuating electricity prices, with integrated scheduling and control enabling coordinated, real-time decisions. This work investigates the trade-off between model fidelity and optimization complexity in dynamic scheduling under integrated dynamic scheduling, using an air separation process in a day-ahead electricity market. We explore mechanistic and typical surrogate dynamic models yielding established optimization formulations combined with standard global and local solution strategies. (Non)linear surrogates are used in full-discretization, formulating (mixed-integer) linear and nonlinear scheduling problems. Local dynamic scheduling with full-order mechanistic models yields superior performance. Conversely, deterministic global dynamic optimization incurs infeasibilities for linear surrogates, and computational intractability for nonlinear surrogates due to branch-and-bound limitations. Instead, stochastic local optimization (multistart) with nonlinear models offers an alternative, delivering high-quality solutions. We conclude that local dynamic scheduling with mechanistic models, and multistart with Hammerstein-Wiener models are preferable for available detailed process models or operational data, respectively.

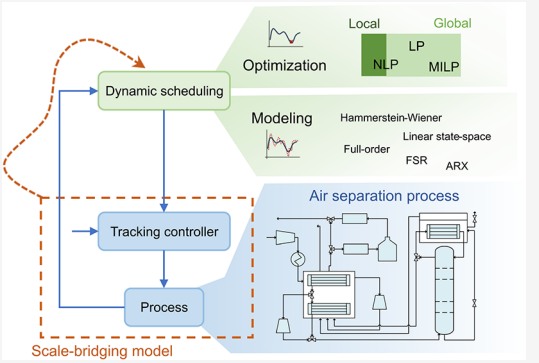

1. INTRODUCTION

Process scheduling is a key strategy for improving efficiency while meeting production goals and process constraints.[1] In the context of demand-response, process scheduling plays a vital role in stabilizing power grids by utilizing economic incentives. In particular, it offers significant economic benefits by enabling electricity-intensive processes to adjust their production in response to fluctuating electricity prices.[2,3] Optimal scheduling methods typically rely on stationary models. However, when the time scales of process dynamics and price variation are comparable, neglecting the process dynamics can lead to inaccuracies, such as infeasible schedules and incorrect cost estimation. Therefore, the integration of process dynamics into the scheduling framework is beneficial, resulting in a dynamic scheduling optimization problem.[4,5]

Under these conditions, strong interaction between hierarchical layers in operational decision-making—distinguished by their characteristic time scales, namely production management (hours to days) and process control (seconds to minutes)[6,7]—emerges, which needs to be addressed to maintain economic performance.[8,9] To this end, integrated scheduling and control frameworks have been developed around the "bottom-up"[9−11] and "top-down"[6] paradigms, with Caspari et al.[12] performing a detailed comparison of the two. The bottom-up approach incorporates scheduling objectives into model-based controllers using an economic cost function.[11] The top-down paradigm or Integrated dynamic scheduling (IDS) retains the hierarchical structure of automation by embedding (open- or closed-loop) plant dynamics into the dynamic scheduling, namely the Dynamic real-time optimization (DRTO) layer.[13,14] This can involve incorporating control laws, such as PID[15,16] or Model predictive control (MPC) optimality conditions,[17,18] to exploit the joint response of the process and its controller. A graphical representation of IDS is given in Figure 1, where besides the general structure, we highlight the modeling and control techniques employed in the present work.

Integrated scheduling and control results in computationally challenging formulations for solving generally nonconvex scheduling problems. As a result, various modeling and optimization techniques have been explored, especially within IDS (see Section 2). A key challenge in developing a solution strategy for IDS is balancing model fidelity and solution accuracy. On one hand, high-fidelity models, namely full-order mechanistic models, enhance accuracy by producing (mostly)

Received: July 2, 2025
Revised: October 12, 2025
Accepted: October 13, 2025
Published: October 29, 2025

https://doi.org/10.1021/acs.iecr.5c02705
Ind. Eng. Chem. Res. 2025, 64, 21641−21657

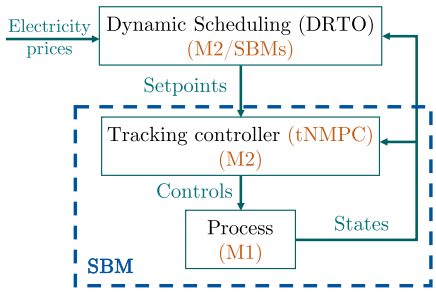

Figure 1. Integrated scheduling and control (IDS). Scale-bridging models (SBMs) are outlined with a dashed line. The modeling and control techniques selected are highlighted in orange. The process models M1, M2, SBMs used at each layer are indicated in parentheses.

feasible schedules that satisfy process constraints and yield precise cost predictions. However, high-fidelity models are characterized by complex nonlinear dynamics, which introduce a large number of variables and nonconvexity in the optimization problem. Since global optimization methods scale poorly—exponentially in the worst case—with dimension, high-fidelity models are often coupled with local optimization methods, which, in contrast, scale better with large, sparse nonlinear problems. On the other hand, local optimization may yield suboptimal results, especially for highly nonconvex scheduling problems. Global optimization can address this limitation but appears intractable when applied to complex, high-dimensional models. This necessitates a trade-off between using high-fidelity models with simplified optimization algorithms, simplified models with global optimization techniques, or simplification in both modeling and optimization—e.g., reduced-order models combined with heuristic search methods. The appropriate choice depends on system dynamics, application, and decision timing constraints. Importantly, such choices must be evaluated at the IDS level, where scheduling-control interactions impact overall performance.

Comparative studies on the trade-off between model fidelity and solution accuracy within IDS remain scarce. Most existing reviews focus on scheduling alone[19−26] overlooking the lower-level control problem, while studies on IDS mainly propose simplifications.[27−30] Pattison et al.[31] present a comparison of modeling techniques and the treatment of process constraints for solving the dynamic scheduling problem within an IDS framework; however, they constrain the comparison to a single type of reduced-order models and a single-shooting solution approach. At the same time, recent advances on dynamic scheduling have yet to be applied in the IDS context. Therefore, a comprehensive comparison of modeling and optimization techniques for dynamic scheduling within IDS is still missing.

Herein, we aim to address this gap by exploring different modeling and optimization combinations for integrated scheduling and control of an Air separation unit (ASU) operating in an electricity market under the IDS paradigm. Our analysis, although not exhaustive, provides insights into scheduling of processes with a highly nonlinear dynamic response and operating and production constraints. On one hand, we consider a high-fidelity full-order ASU model. The high dimensionality of the model calls for local methods to solve the scheduling problem. On the other hand, we employ different types of reduced-order data-driven models, namely a Scale-bridging model (SBM) with discrete-time dynamics (see Section 2). After applying full-discretization, the resulting (Mixed-integer) linear program ((MI)LP) or Nonlinear program (NLP) can be solved with global methods. As simplified models, we investigate Hammerstein-Wiener (HW), Linear state-space (LSS), Autoregressive with extra inputs (ARX), and Finite-step response (FSR) SBMs, offering varying levels of model fidelity. As indication of the model fidelity, we consider a fitting error between process data and predicted model data. Reducing model complexity—by decreasing the number of variables or replacing nonlinear functions with linear ones—although associated with lower prediction accuracy, facilitates optimization while still allowing for global optimization techniques. The resulting schedules are subsequently tracked by MPC using the full-order model. The cost results after tracking are juxtaposed.

In the remainder of this manuscript, we first present a literature review on modeling and optimization techniques for dynamic scheduling (Section 2). In Section 3, we present the concept of IDS and describe the lower-level tracking (Section 3.1) and the upper-level scheduling (Section 3.3) problems implementing SBMs (Section 3.2). Section 4 introduces the ASU case study. Section 5.1 presents the tracking problem formulation. Sections 5.2 and 5.3 give the various scheduling problem formulations resulting from employment of different SBMs. The scheduling formulations determine the IDS scenarios specified in Section 6 and implemented in Section 7. In Section 8, we present the model identification. In Section 9, we compare and discuss the results of the different modeling and optimization scenarios and draw conclusions in Section 10.

2. LITERATURE REVIEW

Next, we review modeling and optimization techniques for dynamic scheduling, emphasizing the predominantly applied approaches for IDS.

Modeling techniques include on the one hand full-order mechanistic models, based on fundamental physical and chemical principles, and on the other hand, model reduction, such as surrogate modeling including data-driven or hybrid approximations.[6,32] We here differentiate between "intrusive"[33−35] and "non-intrusive"[31,36] methods for model order reduction. Intrusive methods retain information on the mechanistic model, e.g., by identifying a set of basis vectors on a low-dimensional linear space.[37,38] Nonintrusive methods generate reduced-order models from time series data without requiring any knowledge of the mechanistic model. In our work, we focus on nonintrusive methods, in particular using a low-order SBM as an input-output representation of the process dynamics,[39] an approach extensively applied to facilitate the solution of the dynamic scheduling problem within IDS.

SBMs are simplified, low-order representations that capture the dynamic behavior of a system at a shorter spatial or time scale and embed it into a higher-level model. In time scale-bridging for scheduling and control, the fast closed-loop process dynamics are approximated by such models, which then connect to the slower scheduling layer by providing set point instead of input trajectories.[6] In general, SBMs do not represent physically meaningful variables, and—in contrast to mechanistic models—are valid only within the operating range of the training data.[40] They require the availability of process or simulation data. In the former case, they can prove of higher fidelity compared to mechanistic models employing simplifi-

https://doi.org/10.1021/acs.iecr.5c02705
Ind. Eng. Chem. Res. 2025, 64, 21641−21657

Table 1. Modeling Approaches Considered in This Work: Advantages and Disadvantages

Model	Full-order mechanistic	Scale-bridging		
		HW		LSS/FSR/ARX
		PWL nonlinearity	Other nonlinearity	
Advantages	•Valid in wide ope-rating range		•Easier to obtain •Fewer variables: smaller-scale optimization	
	•Nonlinear: higher fidelity	•Nonlinear: higher fidelity		•Linear: lower fidelity
	•Plant data not required	• Linear formulation: global optimization	• Reduced-space formulation: global optimization	• Linear: (generally) convex optimization
	•Information on all states			• Local/global optimization
Disadvantages	• Difficult to obtain		• Valid in the data range only	
	• Simplifications: lower fidelity		• Informative plant data required	
			•Input-output information only	
	•Many variables: large scale optimization	• Multiple (hyper-parameters)		•Linear: lower fidelity
	• Nonlinear: nonconvex optimization	• Nonlinear: nonconvex optimization		
	• (Typically) local optimization	• (Typically) local optimization		

cation assumptions. Various types of both continuous- and discrete-time data-driven SBMs have been explored in the literature, ranging from linear parametric[15,39,41] and nonparametric[24,26] models, to block-structured[24,31,42−44] models. Dynamic Mode Decomposition and Recurrent Neural Networks have also been proposed but not yet applied to SBMs, with Tsay and Baldea[32] providing an overview of process system dynamic modeling. For a thorough analysis on model simplification techniques, with applications on IDS, we refer the reader to our recent review by Schulze and Mitsos.[45]

Dynamic scheduling problems are addressed using a range of solution strategies for dynamic optimization, including direct methods,[46] via global optimization,[47,48] decomposition[49,50] and sequential methods, such as single-shooting.[51] Additional strategies include learning-based approaches[52] and heuristic local methods, which explore multiple regions of the solution space by leveraging problem structure,[53] though they often require good initial guesses for convergence.[54] Within the context of IDS, dynamic scheduling problems are predominantly solved using either full-discretization methods combined with either local[5,55−57] or global[58,59] optimization, or single-shooting techniques,[12,60−62] with local methods dominating to address high computational complexity when large nonlinear dynamic models are used. While decomposition approaches[63] and machine learning-based prediction methods[52,64,65] have been proposed, they remain less explored.

Dynamic optimization for scheduling frequently relies on leveraging model structure. A special case of block-structured models widely applied to dynamic scheduling are HW models, which effectively balance model structure simplicity and accurate long-term predictions.[32] Kappatou et al.[66] introduced a framework for solving nonconvex dynamic optimization problems to global optimality by leveraging the structure of HW models and proved convergence based on relaxation theory for ordinary differential equations.[67,68] The resulting NLP is solved globally in a reduced space via a convergent Branch-and-bound B&B algorithm, and a simple numerical integration scheme. We later applied this method to the global dynamic scheduling of an electrochemical process considering a discrete-time dynamic model fitted on open-loop process data.[47] We demonstrated significant cost savings but also experienced poor scalability with respect to problem size. Kelley et al.[24] employed HW models with Piecewise linear (PWL) functions to reformulate the dynamic scheduling as an Mixed-integer linear program (MILP) introducing integer variables, which can be solved to global optimality.

Nonparametric linear time-series FSR models have also been investigated for dynamic scheduling with SBMs describing the closed-loop process response to enable linearization of the optimization problem.[24,25] FSR models can effectively capture complex dynamic process behavior, especially when standard low-order models fail and the model order and time delay are unknown,[7] with increasing identification complexity for a growing number of coefficients.[69,70] Similar to FSR, ARX models have also been considered for linearization of the optimization problem, allowing the global optimization of a Linear program (LP) with reduced computational complexity.[26] In addition, LSS linear models can provide a general formulation for linear model structures. Overall, linear models are expected to describe less accurately nonlinear systems and may therefore require separate treatment of the predicted variables, e.g.,;[26] they allow, however, the use of more sophisticated optimization schemes. A summary of the selected model structures and optimization techniques is given in Table 1. The selection is informed by the literature and our expertise in reduced-order modeling of ASUs, as well as single-shooting and global optimization formulations. Table 1 summarizes the strengths and weaknesses of the considered models.

The aforementioned cases, although investigating dynamic optimization reformulations for scheduling leveraging model structures, they neglect the actual process response after tracking, namely the solution of a lower-level control problem. In our work, we investigate state-of-the-art approaches for modeling in dynamic scheduling coupled with different solution algorithms. Unlike most existing comparative studies, our analysis is performed on the scheduling and control level.

3. INTEGRATED DYNAMIC SCHEDULING

In this section, we present the concept and formulation of the integrated scheduling and control approach of IDS, namely the top-down approach, given in Figure 1. In Section 3.1, we formulate the lower-level Tracking nonlinear model predictive control (tNMPC) problem. Next, we introduce the low-order SBMs used in the DRTO problem of the subsequent case studies (Section 3.2), and finally we incorporate the different

https://doi.org/10.1021/acs.iecr.5c02705
Ind. Eng. Chem. Res. 2025, 64, 21641−21657

modeling techniques to the solution of the DRTO problem (Section 3.3).

In general, IDS employs an upper decision layer to perform scheduling with open-[34,71,72] or closed-[16,18,73] loop process dynamics solving a DRTO problem. The set points are passed to the lower-level controller, which performs real-time adjustments accounting for process feedback. At the lower layer, we perform set point tracking using a tNMPC employing a mechanistic process model (M2). The process feedback is simulated with a (generally) different mechanistic model (M1), which represents the actual process response, introducing a process-model mismatch. Further details on the process-model mismatch are given in the Supporting Information (SI). At the upper layer, we consider both open- and closed-loop models. On one hand, we conduct DRTO with the full-order mechanistic model M2 to capture the open-loop dynamic process response.[71,74] An open-loop dynamic process model does not include a lower-level tNMPC, but may include subordinate regulatory controllers, e.g., PID, to ensure stability. On the other hand, we employ input-output representations of the process response under tracking control.[41] We use data-driven SBMs constructed from simulation data, particularly from closed-loop dynamic optimization in our tNMPC setup.

3.1. Tracking Nonlinear Model Predictive Control. A tNMPC solves an optimal control problem with a tracking objective at discrete time intervals, applying the first control action to the process on a moving horizon fashion.[75]

The problem is formulated as

$$\begin{aligned}
&\min_{\boldsymbol{u}\in\mathcal{U}} \int_{\mathcal{T}_c} (\boldsymbol{x}_p(t) - \boldsymbol{x}_{p,sp}(t))^T Q_x \\
&\quad (\boldsymbol{x}_p(t) - \boldsymbol{x}_{p,sp}(t))\mathrm{d}t \\
&\text{s.t.}\quad \dot{\boldsymbol{x}}(t) = \boldsymbol{f}^{M2}(\boldsymbol{x}(t), \boldsymbol{u}(t)), \\
&\quad \boldsymbol{x}_p(t) \subseteq \boldsymbol{x}(t), \boldsymbol{x}(t) \in \mathcal{X}, \forall\, t \in \mathcal{T}_c, \\
&\quad \boldsymbol{x}(t_0) = \boldsymbol{x}_0
\end{aligned} \tag{1}$$

where $\mathcal{T}_c = [t_0, t_0 + \tau_c]$ is the time window spanning from t_0, and τ_c is the prediction horizon. The controls $\boldsymbol{u}(t) \in \mathbb{R}^{n_u}$, and the states $\boldsymbol{x}(t) \in \mathbb{R}^{n_x}$ have admissible sets $\mathcal{U}$ and $\mathcal{X}$, respectively. A quadratic cost is minimized subject to the process dynamics, given by full order process model M2, with $\boldsymbol{f}^{M2}: \mathbb{R}^{n_x} \times \mathbb{R}^{n_u} \to \mathbb{R}^{n_x}$, the initial conditions $\boldsymbol{x}_0$, and the path constraints given by $\mathcal{X}$ and $\mathcal{U}$. Therein, Q_x is a strictly positive definite weighting matrix, and the subset of the state variables, $\boldsymbol{x}_{p,sp}(t)$, consists the tracking set points. In general, the cost may incorporate an additional term penalizing the control changes between consecutive control steps. In the present application, we omit this term, following our earlier work,[42,62] as abrupt changes in the defined control range do not lead to infeasibilities, and exclude state bounds ($\mathcal{X} = \mathbb{R}^{n_x}$) to avoid a nonsmooth closed-loop response leading to nonsmooth SBMs.

In IDS, a fraction of the tNMPC states corresponds to Scheduling-relevant variables (SRVs).[31] Set points for these SRVs are time-varying, and are provided by the upper scheduling layer, namely $\boldsymbol{v}_{sched,sp}(t) \in \mathbb{R}^{n_v}$. The time-varying set points are the Degrees of freedom (DoFs) of the scheduling problem, namely $\boldsymbol{v}(t) = \boldsymbol{v}_{sched,sp}(t) \in \mathbb{R}^{n_v}$. Then the tNMPC set points are decomposed into the time-varying scheduling solution and constant set points $\boldsymbol{x}_{1,sp}$, giving $\boldsymbol{x}_{p,sp}(t) = [\boldsymbol{x}_{1,sp}\ \boldsymbol{v}(t)]^T$.

The controls $\boldsymbol{u}$ are parametrized as piecewise constant time series with a step change duration Δt_u. The optimal control problem (1) is solved recursively at every sampling period Δt_s, with initial states $\boldsymbol{x}_0$ recursively updated from full-state process feedback (M1 simulation).

3.2. Scale-Bridging Models. To formulate a dynamic scheduling problem, we consider SBMs, denoted by $\boldsymbol{f}^{SBM}$, to describe the closed-loop response of SRVs $\boldsymbol{y}$ to changes in the scheduling inputs $\boldsymbol{v}$ (controller set points), similar to Pattison et al.[31] A general SBM with differential states $\boldsymbol{z}(t)$ is given by

$$\boldsymbol{0} = \boldsymbol{f}^{SBM}(\boldsymbol{z}(t), \dot{\boldsymbol{z}}(t), \boldsymbol{y}(t), \boldsymbol{v}(t)) \tag{2}$$

In practice, simplified inputoutput formulations are often employed. For example, ARX and FSR can be regarded as special cases of SBMs, where the states $\boldsymbol{z}(t)$ are implicit and the dynamics are represented directly through the inputoutput relation. We following formulate the SBMs employed in the subsequent case studies.

3.2.1. Hammerstein-Wiener Models. We begin with Single-input-single-output (SISO) HW models, which in continuous time read

$$\begin{aligned}
&\dot{\boldsymbol{z}}(t) = \mathbf{A}\boldsymbol{z}(t) + \mathbf{B}f_H(v(t)), \quad \boldsymbol{z}(0) = \boldsymbol{z}_0, \\
&y(t) = f_W(h(t)),\ h(t) = \mathbf{C}\boldsymbol{z}(t) + \mathbf{D}f_H(v(t))
\end{aligned} \tag{3}$$

where $v(t) \in \mathbb{R}$ is the single SBM input, $\boldsymbol{z}_0$ is the initial state condition, $h(t) \in \mathbb{R}$ is the single output of the LSS dynamic block and $\mathbf{A} \in \mathbb{R}^{n\times n}$, $\mathbf{B} \in \mathbb{R}^{n\times 1}$, $\mathbf{C} \in \mathbb{R}^{1\times n}$, and $\mathbf{D} \in \mathbb{R}^{1\times 1}$ are linear system matrices. $f_H: \mathbb{R} \to \mathbb{R}$ is the Hammerstein, and $f_W: \mathbb{R} \to \mathbb{R}$ is the Wiener function, while if f_H and f_W are the identity function, eq 3 gives a LSS model. As nonlinear functions, literature has explored PWL, polynomials, sigmoid networks, and Artificial neural networks (ANNs).[12,32,47] System identification tools (e.g., MATLAB) can be exploited for model identification from (plant or simulation) data.

3.2.2. Finite-Step Response Models. Next, we present the linear time-series FSR model. Under the assumption of reached Steady-state (SS) by the end of each scheduling slot—valid for piecewise constant control parametrization, and constant control and price values within a scheduling slot—the FSR reads[76]

$$\hat{y}_{s+k(t-1)} = \hat{y}_{k(t-1)} + S_s\cdot(\hat{v}_t - \hat{v}_{t-1})\ \forall\ t > 1 \tag{4}$$

where $t = 1, 2, ..., n$ indicates the control discretization within the scheduling horizon, and $s = 1, 2, ..., k$ the state discretization within a single control interval. Therein, $\hat{y}$ is the discretized output, and $\hat{v}$ the discretized input, and S is the step response coefficient. The subscripts denote the corresponding time point.

3.2.3. Autoregressive with Extra Inputs Models. Finally, we present ARX in the form of SISO models, inspired from a single set point (input) variation considered in our case studies. Then for a control, and state discretization of $t = 1, 2, ..., n$ and $s = 1, 2, ..., k$, respectively, the ARX model reads

$$A(q)\hat{y}_{s+k(t-1)} = B(q)\hat{v}_{t-n_d} + \hat{e}_{s+k(t-1)} \tag{5}$$

where $A(q)$ is a n_a-degree polynomial giving the number of poles, and $B(q)$ a n_b-degree polynomial giving the number of zeros of the linear model, expressed in a time shift operator

https://doi.org/10.1021/acs.iecr.5c02705
Ind. Eng. Chem. Res. 2025, 64, 21641−21657

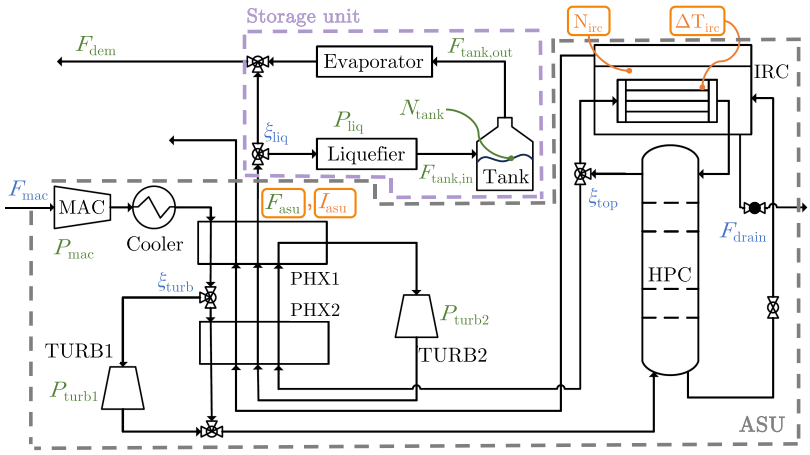

Figure 2. Flowsheet of the ASU. MVs in blue, SRVs in green, and CVs framed in orange. Adapted from Schulze et al.[62] Available under a CC-BY 4.0 license. Copyright 2025 Schulze, Papadimitriou, Kolmer, and Mitsos.

form, q^{-1}. n_d is a delay parameter and $\hat{e}_{s+k(t-1)}$ is a white noise. $\hat{y}$ is the described model output, and $\hat{v}$ the model input. The subscripts denote the corresponding time point.

3.3. DRTO with Different Process Modeling Techniques. In this section, we present formulation approaches of the DRTO problem by employing different dynamic modeling techniques, namely open-loop mechanistic full-order models (Section 3.3.1), and hybrid models (Section 3.3.2).

3.3.1. Dynamic Scheduling with Full-Order Models. The DRTO problem aims to minimize some energy-related operating costs by adjustment of the scheduling inputs or controller set points, namely the optimization variables $\boldsymbol{v}$: $\mathcal{T}_s \to \mathbb{R}^{n_v}$ over a scheduling horizon $\mathcal{T}_s = [0, \tau_s]$, where $\tau_s > \tau_c$ is the scheduling horizon length.

The DRTO problem on a continuous time reads

$$\min_{\boldsymbol{v}(t)\in\mathcal{V}} \int_{\mathcal{T}_s} P(t)\cdot C^e(t)\mathrm{d}t$$

$$\text{s. t.}\quad \mathbf{0} = \boldsymbol{f}^{M2}(\overline{\boldsymbol{z}}(t), \dot{\overline{\boldsymbol{z}}}(t), \overline{\boldsymbol{y}}(t), \boldsymbol{v}(t)),\ P(t) = \overline{y}_1(t),$$

$$\mathbf{0} \geq \boldsymbol{c}(\overline{\boldsymbol{y}}(t), \overline{\boldsymbol{z}}(t), \dot{\overline{\boldsymbol{z}}}(t), C^e(t), t),\ t \in \mathcal{T}_s \qquad (6)$$

where, $\mathcal{V}$ is the admissible set of the controls parametrized as piecewise constant profiles. The costs result from the process power consumption $P(t)$ and the electricity price $C^e(t)$. $\boldsymbol{f}^{M2}: \mathbb{R}^{n_z} \times \mathbb{R}^{n_y} \times \mathbb{R}^{n_u} \to \mathbb{R}^{n_z}$ corresponds to the mechanistic dynamic model M2, where $\overline{\boldsymbol{z}}(t) \in \mathbb{R}^{n_z}$ are the differential states, and $\overline{\boldsymbol{y}}(t) \in \mathbb{R}^{n_y}$ are the model outputs including $P(t)$. The path and point scheduling constraints are given by $\boldsymbol{c}$: $\mathbb{R}^{n_z} \times \mathbb{R}^{n_y} \times \mathbb{R}^{n_u} \to \mathbb{R}^{n_g}$, and mostly represent product quality, inventory and production rate constraints imposed on the SRVs (see Pattison et al.[31]).

3.3.2. Dynamic Scheduling with Hybrid Models. By integrating SBMs (eq 2), given by $\boldsymbol{f}^{SBM}$, with mechanistic submodels, given by $\boldsymbol{f}^{M.S.}$, into the DRTO problem of eq 6, we formulate a dynamic scheduling problem with a hybrid process model. Exemplary hybrid models may include first-principle storage dynamics and SBMs for the main production process, combined through energy and mass balance constraints. SBMs can describe energy consumption, process production, or critical purity levels.[24,42,43,47] The scheduling constraints $\boldsymbol{c}$ of eq 6 are updated to account for the hybrid model states and outputs. Then the DRTO problem with a hybrid process model reads

$$\min_{\boldsymbol{v}(t)\in\mathcal{V}} \int_{\mathcal{T}_s} P(t)\cdot C^e(t)\mathrm{d}t$$

$$\text{s.t.}\quad \mathbf{0} = \boldsymbol{f}^{M.S.}(\overline{\boldsymbol{z}}(t), \dot{\overline{\boldsymbol{z}}}(t), \overline{\boldsymbol{y}}(t), \boldsymbol{v}(t)),\ P(t) = \overline{y}_1(t),$$

$$\mathbf{0} = \boldsymbol{f}^{SBM}(\boldsymbol{z}(t), \dot{\boldsymbol{z}}(t), \boldsymbol{y}(t), \boldsymbol{v}(t)),$$

$$\mathbf{0} \geq \boldsymbol{c}(\boldsymbol{y}(t), \overline{\boldsymbol{y}}(t), \overline{\boldsymbol{z}}(t), \dot{\overline{\boldsymbol{z}}}(t), C^e(t), t),\ t \in \mathcal{T}_s \qquad (7)$$

4. CASE STUDY

We perform IDS on the single-product ASU described by Caspari et al.,[12] presented in Figure 2. The ASU units comprise a main air compressor (MAC), two heat exchangers (PHX1, PHX2), two turbines (TURB1, TURB2), and a high-pressure distillation column (HPC) with an integrated reboiler-condenser (IRC). The nitrogen product is stored in a storage unit consisting of a liquefier, a storage tank, and an evaporator.

The process control (tNMPC) inputs, namely the Manipulated variables (MVs), highlighted in blue in Figure 2, are the molar flow rate F_{mac} of the air feed, the split fraction ξ_{turb} of air flow into TURB1, the split fraction ξ_{liq} of the product stream into the liquefier, the reflux fraction ξ_{top}, and the reboiler liquid drain F_{drain}. The The Controlled variables (CVs), highlighted in orange in Figure 2, are the ASU production rate F_{asu}, the product impurity level I_{asu}, and the IRC tank level N_{irc}, and temperature difference ΔT_{irc} in the IRC. The storage unit is disregarded from the tNMPC, due to fast dynamics compared to the ASU.

The SRVs for upper-layer DRTO, highlighted in green in Figure 2, are the product demand F_{dem}, the MAC power intake P_{mac}, the TURB1 (P_{turb1}) and TURB2 (P_{turb2}) power output, and F_{asu}. Additionally, the liquefier power consumption P_{liq} and the storage tank input ($F_{tank,in}$) and output ($F_{tank,out}$) flow rates, and tank level N_{tank} are SRVs. We note that, in contrast to our previous works,[24,30,43] the product purity is closely tracked, thus I_{asu} is not a part of the SRVs.

5. UPPER- AND LOWER-LEVEL PROBLEM FORMULATION

In this section, we introduce the mathematical formulation of the lower-level tNMPC problem (Section 5.1) and the upper-

https://doi.org/10.1021/acs.iecr.5c02705
Ind. Eng. Chem. Res. 2025, 64, 21641−21657

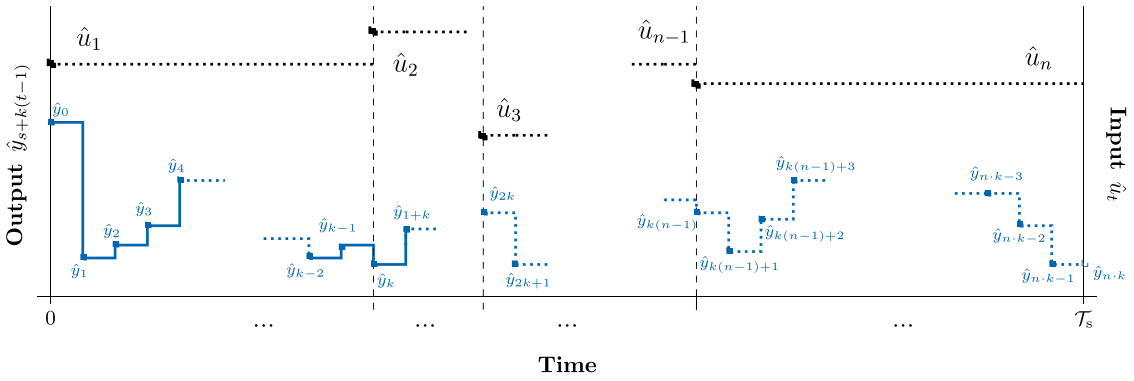

Figure 3. Piecewise constant control and state parametrization and equidistant time discretization for the general case of different control and state discretization schemes.

level DRTO problem considering either a mechanistic (Section 5.2), or a hybrid process model (Section 5.3). The mechanistic process model yields Problem formulation 1, while different surrogate models reformulate the DRTO to Problems 2 to 6.

5.1. Formulation of the tNMPC Problem. First, we present the tNMPC problem formulation according to eq 1 for the ASU case study. We follow our previous work,[42] where the tracking objective is

$$\begin{aligned}&(\boldsymbol{x}_p(t) - \boldsymbol{x}_{p,sp}(t))^T Q_x (\boldsymbol{x}_p(t) - \boldsymbol{x}_{p,sp}(t)) \\ &= \omega_1 \cdot (F_{asu}(t) - F_{asu,sp}(t))^2 + \omega_2 \cdot (I_{asu}(t) - I_{asu,sp})^2 \\ &\quad + \omega_3 \cdot (\Delta T_{irc}(t) - \Delta T_{irc,sp})^2 + \omega_4 \cdot (N_{irc}(t) - N_{irc,sp})^2\end{aligned} \tag{8}$$

The constant weights are given by ω_i, and the controller set points are the time-varying $\boldsymbol{v}(t) = F_{asu,sp}(t)$ and the constant set points $\boldsymbol{x}_{1,sp} = [I_{asu,sp}, \Delta T_{irc,sp}, N_{irc,sp}]$. The controls or MVs are $\boldsymbol{u} = [F_{mac}, \xi_{turb}, \xi_{top}, F_{drain}]^T$. The values of the weights and set points, and the control bounds are given in the SI.

5.2. Problem 1: DRTO with a Full-Order Process Model. First, we consider the full-order, mechanistic dynamic model of the ASU and storage system M2 for DRTO under open-loop process response. We follow eq 6, where $P(t) = P_{asu}(t) + P_{liq}(t)$, with $P_{asu} = P_{mac} - P_{turb1} - P_{turb2}$ and the MVs are $\boldsymbol{u} = [F_{mac}, \xi_{turb}, \xi_{top}, F_{drain}, \xi_{liq}]^T$. The constraints $\boldsymbol{c}$ include bounds on I_{asu}, ΔT_{irc}, N_{irc}, $F_{tank,in}$, $F_{tank,out}$, F_{asu}, and end point constraints on N_{tank}, and N_{irc} to avoid tank depletion at the end of the scheduling horizon. The control bounds and the constraints are given in the SI.

We apply piecewise constant control parametrization and an equidistant control (Δt_u) and state (Δt_s) sampling. Then the large-scale dynamic optimization problem can be solved locally with a local optimization techniques, such as multiple- or single-shooting. In this study, we limit the analysis to single shooting, which is appropriate for the stable dynamic system examined and ensures a reduced number of DoFs. We refer to this DRTO solution approach as Problem 1 (P1).

5.3. DRTO with a Hybrid Process Model. In this section, we present different DRTO formulations for the ASU case study considering a hybrid mechanistic/data-driven process model (see eq 7). The hybrid model includes ASU SBMs, and a linear tank dynamic model combined with mass and energy balance constraints into the DRTO problem. SBMs are identified on closed-loop simulation data for the SRVs F_{asu} and P_{asu} given $F_{asu,sp}$ as input, similar to Schulze et al.,[42] denoted by $f_{SBM,1}$ and $f_{SBM,2}$, respectively

$$\begin{aligned}F_{asu}(t) &= f_{SBM,1}(t, F_{asu,sp}), \\ P_{asu}(t) &= f_{SBM,2}(t, F_{asu,sp})\end{aligned} \tag{9}$$

together with the mechanistic model of the storage system

$$\dot{N}_{tank}(t) = F_{tank,in}(t) - F_{tank,out}(t),\ N_{tank}(0) = N^0_{tank} \tag{10}$$

$$F_{tank,in}(t) = F_{tank,out}(t) + F_{asu}(t) - F_{dem}(t) \tag{11}$$

$$P_{liq}(t) = f_{liq}(F_{tank,in}(t)) \tag{12}$$

Here, we disregard detailed thermodynamic calculations related to eq 12, and express f_{liq} as a linear function of the inlet flow using the polytropic head of the unit α, similar to Kelley et al.[24]

$$P_{liq}(t) = \alpha \cdot F_{tank,in}(t) \tag{13}$$

where α is calculated through fitting of inlet flow and liquefier power process data.

The scheduling problem minimizes the total electricity-related costs

$$\min_{F_{asu,sp} \in \mathbb{F}} \int_{\mathcal{T}_s} (P_{asu}(t) + P_{liq}(t)) \cdot C^e(t) \mathrm{d}t \tag{14}$$

where $\mathbb{F}$ gives the production set point bounds. Additional constraints ensure a tank level within bounds

$$N^{min}_{tank} \le N_{tank}(t) \le N^{max}_{tank} \tag{15}$$

the same storage tank holdup at the beginning and at the end of the day, similar to P1

$$N_{tank}(t = \mathcal{T}_s) = N^0_{tank} \tag{16}$$

and either filling or draining of the storage tank

$$\begin{aligned}&F_{tank,out}(t) + F_{asu}(t) \ge F_{dem}(t), \\ &F_{tank,in}(t),\ F_{tank,out}(t) \ge 0\end{aligned} \tag{17}$$

Although the problem is defined in continuous time, the discrete nature of prices and SBM data motivates a discrete-time DRTO formulation, using discrete-time SBMs and tank dynamics. Tank dynamics are discretized via a forward Euler scheme of discretization step Δt_s, assuming piecewise constant states and controls. Then $F_{tank,in}(t)$, $F_{tank,out}(t)$ remain constant in $(t, t + \Delta t_s]$, and eq 10 is replaced with

https://doi.org/10.1021/acs.iecr.5c02705
Ind. Eng. Chem. Res. 2025, 64, 21641−21657

$$\hat{N}_{\text{tank},i'} = (\hat{F}_{\text{tank,in},i'} - \hat{F}_{\text{tank,out},i'})\Delta t_s + \hat{N}_{\text{tank},i'-1},$$
$$\hat{N}_{\text{tank},0} = N^0_{\text{tank}} \tag{18}$$

where $i' = 1, 2, \ldots$ denotes the state discretization point.

Next, we examine reformulations and optimization techniques for globally solving the discretized DRTO problem using a discretize-then-optimize approach. Section 5.3.1 accounts for nonlinear SBMs, resulting in Problem formulations 2 and 3, while in Section 5.3.2, we incorporate linear SBMs in the DRTO, rendering Problems 4 to 6.

5.3.1. DRTO with Nonlinear SBMs. In this Section, we apply nonlinear HW SBMs for the hybrid ASU model. First, we account for generally nonconvex HW functions (Problem 2). Next, we deal exclusively with PWL static blocks (Problem 3).

5.3.1.1. Problem 2: DRTO with Hammerstein-Wiener SBMs. For the DRTO problem of eqs 9 to 18, we apply HW SBMs (eq 3), expressed in discrete time. Then, the fully discretized problem can be solved using a simultaneous method, resulting in a high-dimensional sparse NLP. To reduce dimensionality, $F_{\text{tank,in}}(t)$ is replaced with $(1 - \xi_{\text{liq}}(t)) \cdot F_{\text{asu}}(t)$. The controls are sampled uniformly over n intervals across the scheduling horizon $\mathcal{T}_s$, each denoted by t, and k piecewise constant states exist in each control interval, each denoted by s, so that $\tau_s/(n{\cdot}k) = \Delta t_s$. The discretization scheme is given in Figure 3. Then we rewrite the DRTO in a reduced-space formulation, to form an NLP of reduced dimensionality

$$\begin{aligned}
\min_{\hat{v}\in\mathcal{V}}\ & \tau_s \cdot \textstyle\sum_{t=1}^{n}\sum_{s=1}^{k} C^{\text{e}}_{s+k(t-1)}\cdot(f_{\text{W},2}(\boldsymbol{c}_2\hat{\boldsymbol{z}}_{2,s+k(t-1)} + d_2\cdot\hat{w}_{2,t}) \\
& + \alpha\cdot(1-\hat{\xi}_{\text{liq},t})\cdot f_{\text{W},1}(\boldsymbol{c}_1\hat{\boldsymbol{z}}_{1,s+k(t-1)} + d_1\cdot\hat{w}_{1,t}))\\
\text{s.t.}\ & \hat{w}_{1,t} = f_{\text{H},1}(\hat{F}_{\text{asu,sp},t}),\ \hat{w}_{2,t} = f_{\text{H},2}(\hat{F}_{\text{asu,sp},t}),\\
& \hat{N}_{\text{tank},n\cdot k} = N^0_{\text{tank}},\ N^{\min}_{\text{tank}} \le \hat{N}_{\text{tank},s+k(t-1)} \le N^{\max}_{\text{tank}},\\
& \forall\, t \in \{1, 2, \ldots, n\},\ s \in \{1, 2, \ldots, k\}
\end{aligned} \tag{19}$$

where $\hat{\boldsymbol{v}} = [\hat{\boldsymbol{F}}_{\text{asu,sp}},\ \hat{\boldsymbol{w}}_1,\ \hat{\boldsymbol{\xi}}_{\text{liq}},\ \hat{\boldsymbol{w}}_2]$, $\mathcal{V} = [F^{\min}_{\text{asu,sp}}, F^{\max}_{\text{asu,sp}}] \times [w_1^{\min}, w_1^{\max}] \times [\xi^{\min}_{\text{liq}}, \xi^{\max}_{\text{liq}}]$, the states $\times\, [w_2^{\min}, w_2^{\max}]$ derive from the linear dynamics

$$\hat{N}_{\text{tank},s+k(t-1)} = (\hat{F}_{\text{asu,sp},t} - \hat{F}_{\text{dem}})\Delta t_s + \hat{N}_{\text{tank},s+k(t-1),-1}$$
$$\hat{N}_{\text{tank},0} = N^0_{\text{tank}} \tag{20}$$

$$\hat{\boldsymbol{z}}_{1,s+k(t-1)} = \boldsymbol{A}_1\hat{\boldsymbol{z}}_{1,s+k(t-1)-1} + \boldsymbol{b}_1\hat{w}_{1,t},$$
$$\hat{\boldsymbol{z}}_{2,s+k(t-1)} = \boldsymbol{A}_2\hat{\boldsymbol{z}}_{2,s+k(t-1)-1} + \boldsymbol{b}_2\hat{w}_{2,t},$$
$$\hat{\boldsymbol{z}}_{1,0} = \hat{\boldsymbol{z}}_1^{\,0},\ \hat{\boldsymbol{z}}_{2,0} = \hat{\boldsymbol{z}}_2^{\,0}\ \forall\, t \in \{1, 2, .., n\},\ s \in \{1, 2, \ldots, k\} \tag{21}$$

and the controls and states are parametrized as

$$\begin{aligned}
&\hat{\boldsymbol{z}}_{1,s+k(t-1)} = [\hat{z}_{1,1,s+k(t-1)} \cdots \hat{z}_{1,l_1,s+k(t-1)}]^{\text{T}} \in \mathbb{R}^{l_1},\ \hat{\boldsymbol{w}}_1 = [\hat{w}_{1,1} \cdots \hat{w}_{1,n}]^{\text{T}} \in \mathbb{R}^n,\\
&\hat{\boldsymbol{z}}_{2,s+k(t-1)} = [\hat{z}_{2,1,s+k(t-1)} \cdots \hat{z}_{2,l_2,s+k(t-1)}]^{\text{T}} \in \mathbb{R}^{l_2},\ \hat{\boldsymbol{w}}_2 = [\hat{w}_{2,1} \cdots \hat{w}_{2,n}]^{\text{T}} \in \mathbb{R}^n,\\
&\hat{\boldsymbol{\xi}}_{\text{liq}} = [\hat{\xi}_{\text{liq},1} \cdots \hat{\xi}_{\text{liq},n}]^{\text{T}} \in \mathbb{R}^n,\ \hat{\boldsymbol{f}}_{\text{asu,sp}} = [\hat{F}_{\text{asu,sp},1} \cdots \hat{F}_{\text{asu,sp},n}]^{\text{T}} \in \mathbb{R}^n
\end{aligned} \tag{22}$$

In eq 20, we have replaced $\hat{F}_{\text{dem},s+k(t-1)}$, with $\hat{F}_{\text{dem}}$, given a constant product demand over time, and we have assumed $\hat{F}_{\text{asu},s+k(t-1)} \simeq \hat{F}_{\text{asu,sp},t}$ to retain linearity of the dynamics. The parametrized and discretized optimization problem with nonconvex objective and constraints, and linear dynamics can then be solved to global optimality with a B&B algorithm following the approach of Kappatou et al.[66] We thereafter refer to eqs 19−21 as Problem 2 (P2). Constraint values for P2 are provided in the SI.

5.3.1.2. Problem 3: DRTO with Hammerstein-Wiener SBMs with Piecewise Linear Nonlinearities. Next, we present the special case of PWL Hammerstein and Wiener nonlinearities in the SBMs (eq 3). Following Kelley et al.,[24,25] we use Special ordered sets of the second type (SOS2) to reformulate the nonlinear functions as mixed-integer linear constraints in the discretized DRTO problem (eqs 9−18), under piecewise-constant state and control parametrization, similar to P2. Therein we introduce the SOS2 variables $\lambda^{\text{H}}_{1,t,j}$, $\lambda^{\text{H}}_{2,t,j}$ for the $\hat{F}_{\text{asu}}$ and $\hat{P}_{\text{asu}}$ Hammerstein functions, respectively, and $\lambda^{\text{W}}_{1,s+k(t-1),j}$, $\lambda^{\text{W}}_{2,s+k(t-1),j}$, for the corresponding Wiener functions. The SOS2 variables are defined for each time point given by $t = 1, 2, \ldots, n$, and $s = 1, 2, \ldots, k$, and each breakpoint $j \in \mathbb{Z}^*$ of the PWL function. Each λ is linked to an integer variable r, which indicates the active interval between consecutive breakpoints, following

$$\lambda^{\text{H}}_{i,t,j} \in [0, 1],\ r^{\text{H}}_{i,t,j} \in \{0, 1\},\ \forall\, i \in \{1, 2\} \tag{23}$$

$$\begin{aligned}
&\sum_{j=1}^{j^{\text{H}}_i} \lambda^{\text{H}}_{i,t,j} = 1,\ \sum_{j=1}^{j^{\text{H}}_i} r^{\text{H}}_{i,t,j} = 2\\
&r^{\text{H}}_{i,t,j} + r^{\text{H}}_{i,t',j} \le 1,\ \forall\, t' \ge t+2,\\
&\lambda^{\text{H}}_{i,t,j} \le r^{\text{H}}_{i,t,j},\ \forall\, i \in \{1, 2\}
\end{aligned} \tag{24}$$

for the Hammerstein, and

$$\lambda^{\text{W}}_{i,s+k(t-1),j} \in [0, 1],\ r^{\text{W}}_{i,s+k(t-1),j} \in \{0, 1\},\ \forall\, i \in \{1, 2\} \tag{25}$$

$$\begin{aligned}
&\sum_{j=1}^{j^{\text{W}}_i} \lambda^{\text{W}}_{i,s+k(t-1),j} = 1,\ \sum_{j=1}^{j^{\text{W}}_i} r^{\text{W}}_{i,s+k(t-1),j} = 2,\\
&r^{\text{W}}_{i,s+k(t-1),j} + r^{\text{W}}_{i,t',j} \le 1,\ \forall\, t' \ge s + k(t-1) + 2,\\
&\lambda^{\text{W}}_{i,s+k(t-1),j} \le r^{\text{W}}_{i,s+k(t-1),j},\ \forall\, i \in \{1, 2\}
\end{aligned} \tag{26}$$

for the Wiener function, where $i = 1$ corresponds to the $\hat{F}_{\text{asu}}$-SBM, and $i = 2$ to the $\hat{P}_{\text{asu}}$-SBM, and j^{H}_i and j^{W}_i is the number of breakpoints of the Hammerstein, and Wiener function, respectively. By interpolating between the breakpoint positions $(\text{bp}^{\text{H}}_{1,j})$ and breakpoint values $(\text{pw}^{\text{H}}_{1,j})$, we obtain the Hammerstein block input and output.

$$\hat{F}_{\text{asu,sp},t} = \sum_{j=1}^{j^{\text{H}}_1} (\lambda^{\text{H}}_{1,t,j}\cdot\text{bp}^{\text{H}}_{1,j}),$$
$$\hat{w}_{1,t} = \sum_{j=1}^{j^{\text{H}}_1} (\lambda^{\text{H}}_{1,t,j}\cdot\text{pw}^{\text{H}}_{1,j}) \tag{27}$$

Similarly for the Wiener block, we obtain

https://doi.org/10.1021/acs.iecr.5c02705
Ind. Eng. Chem. Res. 2025, 64, 21641−21657

$$\hat{h}_{1,s+k(t-1)} = \sum_{j=1}^{j_1^{\mathrm{W}}} (\lambda^{\mathrm{W}}_{1,s+k(t-1),j} \cdot \mathrm{bp}^{\mathrm{W}}_{1,j}),$$

$$\hat{F}_{\mathrm{asu},s+k(t-1)} = \sum_{j=1}^{j_1^{\mathrm{W}}} (\lambda^{\mathrm{W}}_{1,s+k(t-1),j} \cdot \mathrm{pw}^{\mathrm{W}}_{1,j}) \tag{28}$$

where $\hat{h}_{1,s+k(t-1)}$ is the discretized linear block output for the $\hat{F}_{\mathrm{asu}}$-SBM.

For the $\hat{P}_{\mathrm{asu}}$-SBM we similarly retrieve

$$\hat{F}_{\mathrm{asu,sp},t} = \sum_{j=1}^{j_2^{\mathrm{H}}} (\lambda^{\mathrm{H}}_{2,t,j} \cdot \mathrm{bp}^{\mathrm{H}}_{2,j}),\ \hat{w}_{2,t} = \sum_{j=1}^{j_2^{\mathrm{H}}} (\lambda^{\mathrm{H}}_{2,t,j} \cdot \mathrm{pw}^{\mathrm{H}}_{2,j}),$$

$$\hat{h}_{2,s+k(t-1)} = \sum_{j=1}^{j_2^{\mathrm{W}}} (\lambda^{\mathrm{W}}_{2,s+k(t-1),j} \cdot \mathrm{bp}^{\mathrm{W}}_{2,j}),\ \hat{P}_{\mathrm{asu},s+k(t-1)} = \sum_{j=1}^{j_2^{\mathrm{W}}} (\lambda^{\mathrm{W}}_{2,s+k(t-1),j} \cdot \mathrm{pw}^{\mathrm{W}}_{2,j}) \tag{29}$$

An exemplary PWL Hammerstein function of the $\hat{F}_{\mathrm{asu}}$-SBM is visualized in Figure 4, where we note the SOS2 and integer variables.

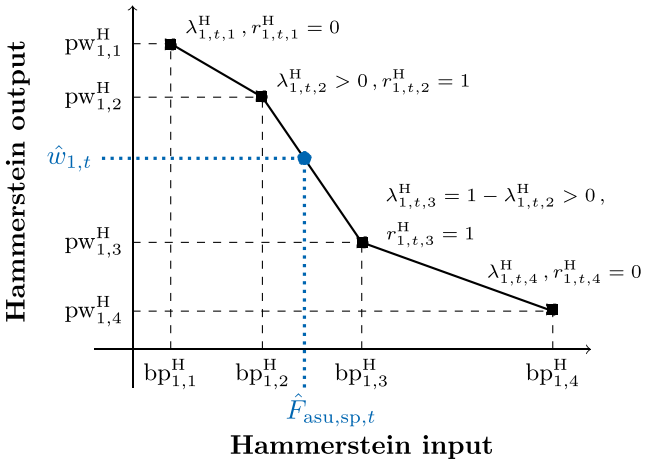

Figure 4. Piecewise linear Hammerstein function with use of SOS2 variables.

We then formulate the discretized DRTO problem in a full space, considering a simultaneous dynamic optimization approach.

$$\min_{\hat{\boldsymbol{v}} \in \mathcal{V}} \tau_{\mathrm{s}} \cdot \sum_{t=1}^{n} \sum_{s=1}^{k} C^{\mathrm{e}}_{s+k(t-1)} \cdot (\hat{P}_{\mathrm{asu},s+k(t-1)} + \hat{P}_{\mathrm{liq},s+k(t-1)}) \tag{30}$$

subject to the HW state constraints of eq 21, and

$$\hat{\boldsymbol{h}}_{1,s+k(t-1)} = \boldsymbol{c}_1 \hat{\boldsymbol{z}}_{1,s+k(t-1)} + d_1 \cdot \hat{w}_{1,t},$$

$$\hat{\boldsymbol{h}}_{2,s+k(t-1)} = \boldsymbol{c}_2 \hat{\boldsymbol{z}}_{2,s+k(t-1)} + d_2 \cdot \hat{w}_{2,t},\ \forall\, t \in \{1, 2, .., n\},\ s \in \{1, 2, ..., k\} \tag{31}$$

the SOS2, and integer variable constraints of eqs 24, 26–27, the tank dynamics of eq 20, and the liquefier and tank constraints

$$\hat{P}_{\mathrm{liq},s+k(t-1)} = \alpha \cdot \hat{F}_{\mathrm{tank,in},s+k(t-1)},$$

$$\hat{F}_{\mathrm{tank,in},s+k(t-1)} + \hat{F}_{\mathrm{asu},s+k(t-1)} \geq 0,\ \forall\, t \in \{1, 2, .., n\},\ s \in \{1, 2, ..., k\}$$

$$\hat{N}_{\mathrm{tank},n \cdot k} = N^0_{\mathrm{tank}},\ \forall\, t \in \{1, 2, .., n\},\ s \in \{1, 2, ..., k\} \tag{32}$$

In eq 30, $\hat{\boldsymbol{v}}$ are the DoFs, namely all the parametrized and discretized (see eq 22) controls and states, the tank flow variables, the SOS2 and integer variables, and $\mathcal{V}$ includes bounds on $\hat{F}_{\mathrm{asu,sp},t}$ and $\hat{N}_{\mathrm{tank},s+k(t-1)}$ of eq 19, the tank flows, namely $\hat{F}_{\mathrm{tank,in},\, s+k(t-1)} \in [0, F^{max}_{\mathrm{tank}}]$, $\hat{F}_{\mathrm{tank,out},s+k(t-1)} \in [0, F^{max}_{\mathrm{tank}}]$, all input, output and states of the SBMs, and the SOS2 and integer variables (eqs 23 and 25). Numerical values of the bounds are provided in the SI. The resulting MILP of eqs 20, 21, 24, 26–32, referenced as Problem 3 (P3), can then be solved to global optimality using a B&B algorithm.

5.3.2. DRTO with Linear SBMs. In this Section, we use LSS SBMs in the hybrid ASU model to formulate the DRTO problem in full (Problem 4) and reduced (Problem 5) space. To improve model accuracy, while confining to linear dynamics, we apply LSS, FSR, and ARX SBMs (Problem 6).

5.3.2.1. Problem 4: DRTO with Linear State-Space SBMs in Full Space. We consider LSS dynamic models for eq 9. The fully discretized problem, can be solved with a simultaneous method, resulting in a high-dimensional LP. The problem adjusts on P3 and reads:

$$\min_{\hat{\boldsymbol{v}} \in \mathcal{V}} \tau_{\mathrm{s}} \cdot \sum_{t=1}^{n} \sum_{s=1}^{k} C^{\mathrm{e}}_{s+k(t-1)} \cdot (\hat{P}_{\mathrm{asu},s+k(t-1)} + \hat{P}_{\mathrm{liq},s+k(t-1)}) \tag{33}$$

subject to the tank and liquefier constraints (20), (32), and the SBM dynamics of F_{asu}

$$\hat{\boldsymbol{z}}_{1,s+k(t-1)} = \boldsymbol{A}_1 \hat{\boldsymbol{z}}_{1,s+k(t-1)-1} + \boldsymbol{b}_1 \hat{F}_{\mathrm{asu,sp},t},\ \hat{\boldsymbol{z}}_{1,0} = \hat{\boldsymbol{z}}^0_1,$$

$$\hat{F}_{\mathrm{asu},s+k(t-1)} = \boldsymbol{c}_1 \hat{\boldsymbol{z}}_{1,s+k(t-1)} + d_1 \cdot \hat{F}_{\mathrm{asu,sp},t},\ \forall\, t \in \{1, 2, .., n\},\ s \in \{1, 2, ..., k\} \tag{34}$$

and P_{asu}

$$\hat{\boldsymbol{z}}_{2,s+k(t-1)} = \boldsymbol{A}_2 \hat{\boldsymbol{z}}_{2,s+k(t-1)-1} + \boldsymbol{b}_2 \hat{F}_{\mathrm{asu,sp},t},\ \hat{\boldsymbol{z}}_{2,0} = \hat{\boldsymbol{z}}^0_2,$$

$$\hat{P}_{\mathrm{asu},s+k(t-1)} = \boldsymbol{c}_2 \hat{\boldsymbol{z}}_{2,s+k(t-1)} + d_2 \cdot \hat{F}_{\mathrm{asu,sp},t},\ \forall\, t \in \{1, 2, .., n\},\ s \in \{1, 2, ..., k\} \tag{35}$$

where the DoFs $\hat{\boldsymbol{v}}$ include the parametrized and discretized (see eq 22) controls and states, the tank flow variables, and $\mathcal{V}$ is similar to P3, excluding SOS2 and integer variables. Numerical values of bounds are given in the SI. Equations 20, and 32–35 comprise Problem 4 (P4).

5.3.2.2. Problem 5: DRTO with Linear State-Space SBMs in Reduced Space. To decrease dimensionality of P4, we follow Section 5.3.1, and replace $F_{\mathrm{tank,in}}$ with $(1 - \xi_{\mathrm{liq}}(t)) \cdot F_{\mathrm{asu}}(t)$. We maintain the control and state parametrization of P2, and rewrite the DRTO in reduced space to obtain a low-dimensional NLP with linear dynamics

$$\begin{aligned} \min_{\hat{\boldsymbol{v}} \in \mathcal{V}}\ & \tau_{\mathrm{s}} \cdot \sum_{t=1}^{n} \sum_{s=1}^{k} C^{\mathrm{e}}_{s+k(t-1)} \cdot (f_{\mathrm{W},2}(\boldsymbol{c}_2 \hat{\boldsymbol{z}}_{2,s+k(t-1)} + d_2 \cdot \hat{F}_{\mathrm{asu,sp},t}) \\ & + \alpha \cdot (1 - \hat{\xi}_{\mathrm{liq},t}) \cdot f_{\mathrm{W},1}(\boldsymbol{c}_1 \hat{\boldsymbol{z}}_{1,s+k(t-1)} + d_1 \cdot \hat{F}_{\mathrm{asu,sp},t})) \\ \text{s. t.}\ & N^{\min}_{\mathrm{tank}} \leq \hat{N}_{\mathrm{tank},s+k(t-1)} \leq N^{\max}_{\mathrm{tank}}, \\ & \hat{N}_{\mathrm{tank},n \cdot k} = N^0_{\mathrm{tank}},\ \forall\, t \in \{1, 2, .., n\},\ s \in \{1, 2, ..., k\} \end{aligned} \tag{36}$$

where $\hat{\boldsymbol{v}} = [\hat{F}_{\mathrm{asu,sp}}, \hat{\boldsymbol{\xi}}_{\mathrm{liq}}]$, $\mathcal{V} = [F^{\min}_{\mathrm{asu,sp}}, F^{\max}_{\mathrm{asu,sp}}] \times [\xi^{\min}_{\mathrm{liq}}, \xi^{\max}_{\mathrm{liq}}]$, and the states derive from the linear dynamics of eqs 20, 34–36. The parametrized and discretized NLP can then be solved globally with B&B following Kappatou et al.[66] We thereafter refer to eqs 20, 34–36, as Problem 5 (P5).

5.3.2.3. Problem 6: DRTO with Various Linear SBMs in Full Space. Next, we focus on improving model accuracy while preserving linearity of the DRTO. To achieve this, we employ linear LSS, ARX, and FSR SBMs to capture the ASU power consumption and production flow rate F_{asu} dynamics. For

https://doi.org/10.1021/acs.iecr.5c02705
Ind. Eng. Chem. Res. 2025, 64, 21641−21657

Table 2. Summary of DRTO Problem Formulations[a]

DRTO strategy	Problem formulation	Number of DoFs	Model			Solution	
			type	SRVs	name	method	guarantee
P1-SS[b]	NLP, RS	120	Full-order mechanistic	N/A	M2	Single-shooting	Local
P1-R[b]							
P2	NLP, RS	96	HW-ANN	F_{asu}, P_{asu}	M3, M6	Full-discretization	Global
P3	MILP, FS	12520	HW-PWL		M4, M7		
P4	LP, FS	4070	LSS		M5, M8		
P5	NLP, RS	48	LSS		M5, M8		
P6	LP, FS	4070	ARX, LSS, FSR	F_{asu}, P_{turb1}, P_{mac}, P_{turb2}	M8−M11		
IPOPT-1[c]	NLP, RS	96	HW-ANN	F_{asu}, P_{asu}	M3, M6	Full-discretization	Local
IPOPT-2[c]							
IPOPT-3[c]							
IPOPT-4[c]							

[a]RS refers to reduced- and FS to full-space formulation. SRVs are scheduling-relevant variables described by scale-bridging models. All DRTO solutions are tracked by tNMPC with the full-order model M2. [b]R: random initialization, SS: initialization at optimal steady-state. [c]Different solutions of multistart with IPOPT considering the formulation of P2.

improved predictive performance, P_{asu} is decomposed into submodels of the power contributions, namely an LSS model for P_{mac}, an ARX model for P_{turb1}, and an FSR model for P_{turb2}. We emphasize that the model decomposition introduced here is not intended to address poor predictive performance of nonlinear SBMs on P_{asu}, but rather to enhance the predictive accuracy of power consumption when using linear SBMs. We additionally consider an LSS SBM for F_{asu}. The model selection follows identification preprocessing explained in Section 8. Then, we reformulate P4 and obtain the following LP

$$\min_{\hat{\nu}\in\mathcal{V}} \tau_s \cdot \sum_{t=1}^{n}\sum_{s=1}^{k} C^{e}_{s+k(t-1)} \cdot (\hat{P}_{mac,s+k(t-1)} - \hat{P}_{turb1,s+k(t-1)} - \hat{P}_{turb2,s+k(t-1)} + \hat{P}_{liq,s+k(t-1)}) \tag{37}$$

subject to the tank and liquefier constraints (20), (32), the LSS dynamics of F_{asu} of eq 34, and P_{mac}

$$\hat{z}_{3,s+k(t-1)} = A_3 \hat{z}_{3,s+k(t-1)-1} + b_3 \hat{F}_{asu,sp,t},\ \hat{z}_{3,0} = \hat{z}^{0}_{3},$$
$$\hat{P}_{mac,s+k(t-1)} = c_3 \hat{z}_{3,s+k(t-1)} + d_3 \cdot \hat{F}_{asu,sp,t},\ \forall\, t \in \{1, 2, .., n\},\ s \in \{1, 2, ..., k\} \tag{38}$$

the ARX dynamics (eq 5) for P_{turb1}

$$a_1 \hat{P}_{turb1,s+k(t-1)} + a_2 \hat{P}_{turb1,s+k(t-1)-1} + ... + a_{n_a+1} \hat{P}_{turb1,s+k(t-1)-n_a} = b_1 \hat{F}_{asu,sp,t-n_d} + b_2 \hat{F}_{asu,sp,t-1-n_d} + ... + b_{n_b} \hat{F}_{asu,sp,t-n_b-n_d} + \hat{e}_{s+k(t-1)},\ \forall\ t \in \{1, 2, ..., n\},\ s \in \{1, 2, ..., k\} \tag{39}$$

and the FSR model (eq 4) of P_{turb2}

$$\hat{P}_{turb2,s+k(t-1)} = \hat{P}_{turb2,k(t-1)} + S_s \cdot (\hat{F}_{asu,sp,t} - \hat{F}_{asu,sp,t-1}),\ \forall\ t \in \{2, .., n\},$$
$$\hat{P}_{turb2,s} = \hat{P}^{0}_{turb2},\ \forall\ s \in \{1, 2, ..., k\} \tag{40}$$

where $\hat{P}^{0}_{turb2}$ is the power output of TURB2 at steady state. The DoFs $\hat{\nu}$ and bounds in $\mathcal{V}$ follow P4, with constraint values provided in the SI. We refer to eqs 20, 32, 34, 37−40, as Problem 6 (P6).

6. SCENARIO CONFIGURATION AND PROBLEM SETUP

In this Section, we specify the scenarios comparing IDS for the ASU case study and describe the operational setup. We employ tNMPC, following Section 5.1, and track the solutions of the upper-level DRTO. To investigate the trade-off between model fidelity and optimization complexity, we first perform DRTO with a full-order model (M2) and local optimization (P1) (Section 5.2). We examine the solution sensitivity to optimization initialization, employing both a naive random (P1-R) initialization and a warm-start initialization at the optimal SS (P1-SS) (see SI). Next, we consider surrogate modeling coupled with deterministic global optimization, following Section 5.3. We explore high-fidelity HW models (M3&M6) solving an NLP (P2) and special-case HW models of lower accuracy (M4&M7) formulating an MILP (P3) to facilitate computations. We additionally consider local solutions of P2 provided through multistart (IPOPT-1 to IPOPT-4) to investigate local optimization with a high-fidelity SBM. Further model simplification using LSS models (M5&M8) enables the solution of an LP in a full (P4) or an NLP in a reduced space (P5) to examine the effect of linear dynamics and solution space on computational demands and schedule feasibility. To improve model accuracy while preserving linearity, i.e., low computational demand, we use linear submodels (M8−M11) to solve an LP in full space (P6). To offer a benchmark for comparison, we perform optimal SS operation at maximum level of impurities (1500 ppm) and nominal production rate (20 mol/s), minimizing the total energy consumption. To quantify the error between M1 and M2, we calculate SS energy and cost results for both process models (SS-M1 and SS-M2). As a reference, we consider SS-M1 representing the actual process operation at optimal SS. In total, we analyze 11 case studies, differentiating between the DRTO, denoted by the problem number (e.g., P2), and the corresponding tNMPC problem, denoted by the problem number-NMPC (e.g., P2-NMPC). A summary of the DRTO case studies addressed is given in Table 2. A description of the models considered is given in Section 8.

To solve the IDS problem, we consider a single-day scheduling horizon (τ_s = 24 h) employing single-day Day-ahead (DA) electricity prices that represent extreme price fluctuations of the year 2023 based on Papadimitriou et al.[77] In

https://doi.org/10.1021/acs.iecr.5c02705
Ind. Eng. Chem. Res. 2025, 64, 21641−21657

all tNMPC and DRTO problems, the piecewise constant states are equidistantly discretized using Δt_s = 5 min. For the piecewise constant controls, tNMPC uses the same control and state discretization, namely Δt_u = 5 min. To ensure comparability, we account for the same control discretization of Δt_u = 1 h in all DRTO problems, leading to n = 24 and k = 12 for P2 to P6.

7. IMPLEMENTATION

We implement the tNMPC algorithm (see eqs 1 and 8) in Python 3.6 using the open-source framework Dynamic Optimization Software (DyOS),[78] which employs the DAE integrator NIXE[79] and the NLP solver SNOPT[80] to track the solutions of P1 to P6. The optimality and feasibility tolerance employed in SNOPT is 10^{-4} and the integration tolerance set in NIXE is set to 10^{-5}. Next, we implement the DRTO problem in DyOS considering a mechanistic process model (P1), with tolerances set to 10^{-3} (optimality), 10^{-4} (feasibility), and 10^{-5} (integration). The full-order models M1 and M2 are written in Modelica and accessed through a Functional Mockup Unit (FMU). The computations are executed on a server with Intel XeonE5−2640 v3 CPU @ 2.60 GHz with 128 GB RAM. The DRTO problems P2 and P5 are implemented on MC++ and solved with our in-house open-source software for deterministic global optimization, MAiNGO,[81] using a B&B algorithm based on McCormick relaxations,[82−84] with a relative optimality tolerance of 10^{-3}. Therein, we use IPOPT[85] to perform multistart and to solve the upper-bounding problem in the B&B and CPLEX (IBM Corporation) for the lower-bounding problem. Solutions of multistart for P2 (IPOPT-1 to IPOPT-4) are additionally tracked with DyOS for comparison. The ANN functions are accessible using the toolbox for machine learning models for optimization MeLOn.[86] We use 20 cores of a CLAIX-2023 node of the high-performance computer of RWTH Aachen University for optimization using the parallel implementation of MAiNGO. During preprocessing, we perform 20 local searches. We further implement the DRTO (MI)LPs P3, P4 and P6 on GAMS (GAMS Development Corp.), which we solve on 14 cores of a server with Intel XeonGold 5117 CPU @ 2.00 GHz with 320 GB RAM using CPLEX (IBM Corporation), with a relative optimality tolerance of 10^{-3}. All DRTO problems are solved with a maximum wall-clock time limit of 24 h considering the computational limitation stemming from the daily update of DA electricity prices.

8. SCALE-BRIDGING MODEL IDENTIFICATION

We generate test and training data from tNMPC tracking the SRVs, following the framework of Pattison et al.[31] The data are used to identify and validate LSS and SISO HW models of the ASU production rate F_{asu}, and power demand P_{asu}, and FSR, LSS and ARX models for F_{asu}, and the power demand of each unit separately (P_{mac}, P_{turb1}, P_{turb2}) using $F_{asu,sp}$ as input, similar to Schulze et al.[62] Linear submodels of the ASU power consumption, are selected to address the poor fit of linear models to the total power consumption P_{asu} directly. The data, hyperparameter and model selection procedure are given in the SI. The identification leads to LSS models for F_{asu} (M8), P_{asu} (M5), and P_{mac} (M9), HW models with either ANNs (M3 for P_{asu} and M6 for F_{asu}) or PWL (M4 for P_{asu} and M7 for F_{asu}) nonlinear blocks, an FSR for P_{turb2} (M10), and an ARX for P_{turb2} (M11).

The model validation Normalized root mean squared error (NRMSE) results are provided in Table 3, where we also note

Table 3. SBM Identification Results[a]

Variable	Model	Type	Input NL	Output NL	Test fit
P_{asu}	M2	FOM[b]			**96.2%**
	M3	HW	ANN	ANN	**90.0%**
	M4	HW	PWL	PWL	**89.5%**
	M5	LSS			85.4%
F_{asu}	M2	FOM[b]			**99.9%**
	M6	HW	ANN	ANN	99.3%
	M7	HW	PWL	PWL	99.5%
	M8	LSS			99.3%
P_{mac}	M9	LSS			87.6%
P_{turb1}	M10	ARX			92.6%
P_{turb2}	M11	FSR			96.1%

[a]The best performing values are given in **bold**. [b]Full-order mechanistic.

the model accuracy of the SBMs and the full-order model M2 calculated from the process response on the validation data set, as explained in the SI. Test errors ranging from 1−12% resemble previous works on data-driven modeling for ASUs.[24,32,42] For P_{asu} and F_{asu}, the fitting improves with the complexity of the model, namely from LSS models to HW models with PWL, and ANNs (except M7). The test fit for P_{asu} is 96.2%, and for F_{asu} 99.9%, both exceeding the values reported in Table 3, confirming the higher fidelity of M2. Models M6 to M8 exhibit nearly identical performance, indicating the possibility of using simpler (linear) models for F_{asu} without significant loss of accuracy. Table 3 highlights the improved predictive performance of the power submodels compared to the P_{asu} LSS model. The results diverge when P_{asu} is represented by nonlinear HW models.

9. RESULTS AND DISCUSSION

In this section, we evaluate the process performance at optimal SS and assess the effect of process-model mismatch (Section 9.1). Next, we present the DRTO results under different formulations and solution approaches (Section 9.2) and evaluate the results after tracking (Section 9.3). Finally, we give the schedules and cost saving from solving the nonconvex DRTO with multistart. In Table 7, we summarize the final cost reduction after tracking for all DRTO solution strategies implemented, together with information on the problem and models used, and constraint violation information. Further results such as tables and plots, are provided in the SI.

9.1. Optimal Steady-State Operation. In Table 4, we list the energy demand, cost and tank content at the end of the day (in terms of deviation from the desired value) at optimal steady-state operation of 20 mol/s nitrogen production rate. At the reference operating scenario (SS-M1), the total energy demand is 7.37 kWh and the costs related to the DA prices are

Table 4. Results of Steady-State Operation

Operating strategy	Energy demand (kWh)	Relative tank content (%)	Absolute costs (€)	Relative costs (%)
Reference (SS-M1)	7.37	0.0	701	0.0
SS-M2	7.12	0.0	678	−3.4

https://doi.org/10.1021/acs.iecr.5c02705
Ind. Eng. Chem. Res. 2025, 64, 21641−21657

701 € for a single day of operation. Thereafter, we compare the energy and cost results over the reference values in terms of relative deviation (%). We additionally compute the optimal SS operation by open-loop offline optimization with the mechanistic model M2 (SS-M2) and compare the results. SS-M2 predicts 3.4% lower energy demand and cost compared to SS-M1. In terms of cost calculations, the error is notable, as it falls within the range of the energy consumption increase observed during scheduling (6 to 8%), discussed later. However, the M2-M1 model mismatch (see Table 3) remains below the fitting errors of the power SBMs (10 to 15%) (see Section 8) and does not significantly affect the control performance of tNMPC (see Zagrobelny et al.[87]). Supporting calculations based on a key performance indicator for MPC prediction accuracy are provided in the SI. Overall, the observed mismatch is within commonly accepted limits and does not favor a certain modeling technique.

9.2. DRTO under Different Reformulation Strategies. Information on the size of each DRTO problem is given in Table 2. The type and number of DoFs and constraints is provided in the SI. We highlight that reduced-space formulations (P2, P5) can substantially decrease the number of optimization variables (up to 99.6%) and constraints (up to 95.1%) compared to full-space formulations (P3, P4, P6) and optimization with the full-order model (P1). While P4 and P5 use the same LSS models, the reduced-space formulation results in an NLP due to the nonlinearity introduced by the term $(1 - \xi_{liq}(t)) \cdot F_{asu}(t)$. Between all formulations, only P3 includes integers due to the SOS2 variables, resulting in an MILP. We indicate that P4 and P6 are of the same problem type, use linear SBMs and are of similar size. However, P6 uses submodels for the power consumption, offering higher prediction accuracy (Table 3).

Next, we present cost reduction results for local (P1) and global (P2 to P6) dynamic optimization of the DRTO problem, in Table 5, ranging from 4.7 to 9.4%. We note that

Table 5. Results of DRTO[a]

DRTO strategy	Relative costs (%)	Relative optimality gap (%)	Solution time (min)
P1-SS	**−9.4**	N/A	30
P1-R	**−9.4**	N/A	38
P2	**−6.8**	147.6	1440
P3	−6.2	1.9	1440
P4	−4.7	0.1	1
P5	−4.8	9.2	1440
P6	−5.5	0.1	1

[a]The best performing values are given in **bold**.

P1 produces higher cost reduction compared to P2 to P6, which can be explained by the process-model mismatch. However, optimization initialization does not exhibit any effect in the cost results of P1-SS and P1-R, with both cases reaching 9.4% savings and similar scheduling profiles. Between the global DRTO solutions, P2 and P3, with nonlinear models applied produce higher economic savings. P4 and P5 that use the same process model but consider solution in full and reduced space, respectively, produce similar cost results. Among the two cases of DRTO with linear models in full space, namely P4 and P6, P6 with higher model predictive performance achieves a greater cost reduction.

In all cases, optimization is terminated after optimality tolerance is reached or after 24 h of computations. The latter is the case of MILPs and NLPs (P2, P3, P5), while LPs (P4, P6) and DRTO with the full-order model using single-shooting (P1) are solved in a couple minutes, offering a distinct speed-up on the DRTO solution. At the same time, solving P2 with a B&B algorithm results in a large optimality gap of 147.6% at the end of 24 h of computations, indicating weak relaxations, and practically intractable performance. Weak relaxations for P2 are a result of the highly nonconvex equality constraints representing the ANNs, namely the nonlinear Hammerstein and Wiener terms (see eq 19). This effect is not pronounced in the MILP of P3 or the NLP of P5, where the SBMs are linear and nonlinear constraints have been replaced with linear ones. Further information on the relaxations for global dynamic scheduling with HW models is given in the SI.

The convergence of the upper and lower bound for P2 is given in Figure 5. There we additionally indicate the scaled objective value of a few local solutions obtained with multistart at the preprocessing step, ranging from 6.536 to 7.365 kWh.

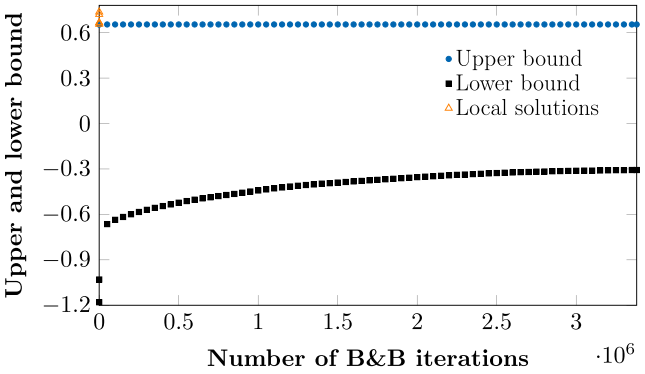

Figure 5. Convergence of B&B algorithm for P2. Local solutions refer to preprocessing with multistart.

9.3. IDS Performance after Tracking. In Table 6, we present the energy consumption results of problems P1 to P6

Table 6. Tracking Performance Results[a]

tNMPC strategy	Relative energy (%)	Relative tank content (%)	Relative costs (%)	Impurities exceeded?
P1-SS-NMPC	6.1	0.4	**−5.3**	No
P1-R-NMPC	6.1	0.4	**−5.3**	No
P2-NMPC	6.2	0.4	**−5.2**	No
P3-NMPC	5.8	0.4	−4.1	No
P4-NMPC	6.2	0.3	−3.5	Yes
P5-NMPC	7.5	0.4	−5.0	Yes
P6-NMPC	7.3	0.4	−5.1	Yes

[a]The best performing values are given in **bold**.

after tracking of the DRTO solution. There, we indicate the final storage tank holdup at the end of the scheduling horizon compared to N^0_{tank} and violations in the product purity during tracking. The relative cost results incorporate the final tank holdup mismatch similar to Schulze et al.[62] All scenarios produce energy demands and a final tank holdup higher than the optimal steady state by 5.8 to 7.5% and 0.3 to 0.4% respectively. All problems that consider linear dynamics (P4 to P6) result in impurity constraint violations after tracking of the solution, while when nonlinear dynamics are considered, the

https://doi.org/10.1021/acs.iecr.5c02705
Ind. Eng. Chem. Res. 2025, 64, 21641−21657

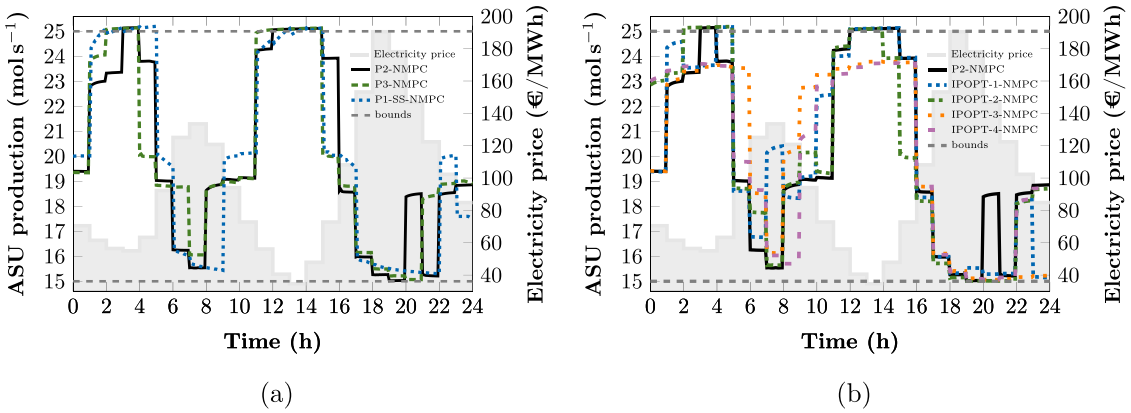

Figure 6. Closed-loop process response of the ASU production rate under IDS. (a) Cases of global dynamic scheduling, (b) Cases of multistart.

Table 7. Economic Performance Summary of All Ids Case Studies after Tracking[a]

DRTO	Problem	Model		Solution	Relative	Impurity
strategy	formulation	type	number	guarantee	costs (%)	exceeded?
SS-M1	N/A	Process	N/A	N/A	0.0	No
P1-SS[b]	NLP, RS	Full-order mechanistic	1	Local	**−5.3**	**No**
P1-R[b]					**−5.3**	**No**
P2	NLP, RS	HW-ANN	2	Global	**−5.2**	**No**
P3	MILP, FS	HW-PWL			−4.1	No
P4	LP, FS	LSS			−3.5	Yes
P5	NLP, RS	LSS			−5.0	Yes
P6	LP, FS	ARX, LSS, FSR	4	Global	−5.1	Yes
IPOPT-0[c]	NLP, RS	HW-ANN	2	Local	**−5.2**	**No**
IPOPT-1[c]					−4.5	No
IPOPT-2[c]					−4.9	No
IPOPT-3[c]					−4.6	No
IPOPT-4[c]					−4.0	No

[a]The best performing results are given in **bold**. [b]R: random initialization, SS: initialization at optimal steady-state [c]Different solutions of multistart with IPOPT considering the formulation of P2.

impurity level remains within bounds (P1 to P3). Similar results of impurity specification violation during tracking have been reported in literature when the schedule is determined through static modeling.[31] In our case, though the impurity levels have not been explicitly modeled. In contrast, the results suggest capturing the dynamic response of the impurity level (similar to the other SRVs), when linear SBMs are used for reduced-order modeling. P1-SS-NMPC and P1-R-NMPC reveal the same cost savings, which are the highest among all case studies, indicating that control initialization and the process-model mismatch has minimal effect on the final results. Between the global optimization DRTO scenarios, P3-NMPC provides the highest cost reduction of 5.2%, almost as good as P1-SS-NMPC, without exceeding impurity limits.

Figure 6a shows the closed-loop response of the production rate of P1-SS-NMPC, P2-NMPC and P3-NMPC. There we note similar fluctuation patterns following the price variation, with higher deviation toward the end of the horizon when terminal constraints are applied. Although, the solution employing the mechanistic model implies high to low production (an vice versa) shifts over the nominal production rate, similar to previous works on ASU scheduling,[28,62] such a shift over the nominal production does not necessarily occur in the solution of P2 and P3, where reduced-order SBMs are used.

9.4. Nonconvex DRTO with Multistart. In Figure 5, we illustrate the evolution of the upper and lower bounds across iterations obtained by solving P2 with B&B. Notably, the final objective value is already achieved during the preprocessing phase via multistart, namely from IPOPT solution IPOPT-0, indicating that B&B does not yield a better solution in this case under the computational time limitations. However, the lower bound improves steadily until B&B ultimately certifies optimality. Although the confidence interval of optimality is large, a general trend on the lower and upper bound evolutions is observed. In the end, the upper bounding solution provides the schedule for tNMPC, similar the rest of the methods that terminate before reaching the desired optimality gap. Given that the solution is already found during preprocessing, we examine alternative solutions generated through multistart and their corresponding performance after tracking. These solutions represent reoptimization of problem P2 in high frequency. For this analysis, we focus on the most accurate nonlinear models identified, specifically M3 and M6, along with DRTO formulation P2.

Relative cost and energy consumption before tracking for several multistart solutions is given in the SI, while the post-tracking results are provided in Table 7. Overall, the savings after tracking lie between 4.0 to 5.2%. This notable deviation highlights the multimodal nature of the problem, indicating that local optimization with nonlinear reduced-order models

https://doi.org/10.1021/acs.iecr.5c02705
Ind. Eng. Chem. Res. 2025, 64, 21641−21657

may yield suboptimal solutions. Nevertheless, improved results can be achieved through search space exploration. Importantly, in all multistart cases, the impurity level remains within acceptable limits, underscoring the benefits of using a nonlinear, high-accuracy model of the closed-loop process response.

Figure 6b illustrates the ASU production flow response after tracking for different schedules obtained through solution of P2 with multistart. It is worth noting that, although different multistart solutions, e.g., IPOPT-1 and IPOPT-3, yield similar cost reductions, their resulting scheduling profiles vary significantly, highlighting the nonconvex nature of the problem. We raise attention to the varying fluctuating behavior at the end of the scheduling horizon, stemming from fulfilling the end point storage constraints.

Finally, we summarize the modeling and optimization results for dynamic scheduling in Figure 7. The figure shows the optimality guarantee as the global optimality gap relative to the fidelity of the model used in the scheduling problem. Local optimization results, are displayed separately in the upper part of the graph to indicate the absence of a global optimality guarantee. When multiple SBMs are applied, only the lowest-fidelity model is reported. Solution approaches are grouped according to the corresponding NMPC results. We observe that low-fidelity linear models, regardless of the optimality guarantee, lead to impurity violations (off-spec production), whereas nonlinear models maintain schedule feasibility. Overall, greater cost reduction is associated with higher model accuracy, while the influence of optimization rigor is less pronounced.

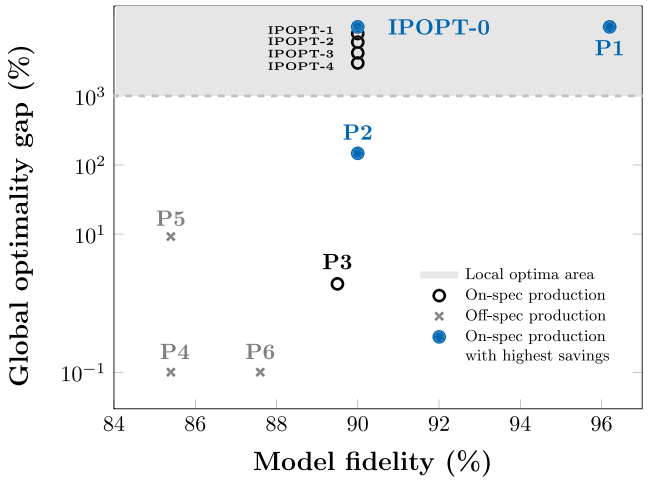

Figure 7. Optimality gap over model fidelity for scheduling strategies. The shaded area marks local optima without global guarantees. Solutions are grouped by cost savings and impurity violation after tracking.

10. CONCLUSIONS AND OUTLOOK

We investigate the operation of an ASU integrated into a DA electricity market under the IDS paradigm. We seek to determine whether high-fidelity models paired with local optimization or low-order data-driven models combined with global optimization offer superior performance in dynamic scheduling. To this end, we implement tNMPC at the lower control level and DRTO at the upper operational level. We explore various process modeling and optimization strategies for DRTO and compare the results after tracking (Table 7).

At the DRTO level, we first consider a high-fidelity full-order model of the ASU. The resulting large-scale NLP can be solved with a local optimization method, such as single-shooting. Next, we explore simpler nonlinear HW models with discrete-time dynamics and employ full-discretization to solve an NLP or an MILP to global optimality. To reduce computational cost, we further simplify the SBMs considering linear ARX, LSS and FSR models. To maintain predictive accuracy with linear models, we perform, submodel decomposition for ARX and FSR. After full-discretization an LP or NLP is solved globally. Additionally, we explore the performance of single-shooting for different initialization strategies, compare global optimization in a full versus a reduced space, and asses local optimization with multistart to solve the nonconvex scheduling problem under nonlinear SBMs. Overall, we consider three problem classes, namely LP, MILP and NLP, derived from six different SBM types, namely full-order, HW with ANNs or PWL functions, LSS, ARX, and FSR.

Full-order process models demonstrate clear advantages over low-order data-driven models, primarily due to their access to all DoFs and constraint-related variables of the lower-level problem, despite exhibiting some process-model mismatch (~4%) and no closed-loop response representation. Notably, the most accurate nonlinear surrogate models with global optimization yield similar scheduling outcomes to mechanistic models with local optimization, suggesting that model fidelity plays a critical role. These are nonlinear reduced-order models, namely the HW with submodel prediction errors varying from 1 to 10%. Furthermore, both local open-loop optimization and nonconvex global dynamic scheduling with SBMs show robustness to initialization. In contrast, linear SBMs often fail to capture essential nonlinear dynamics, leading to constraint violations during tracking. While this behavior should be expected for highly nonlinear dynamic systems, like the ASU operating under soft-constrained tNMPC, it might be less pronounced for systems with a lower degree of nonlinearity or completely addressed with hard-constrained tNMPC or explicit consideration of the impurity response on the scheduling layer. However, the latter entails difficulties, such as in the SBM identification process. Although global dynamic scheduling remains computationally intractable due to B&B limitations, multistart local scheduling with nonlinear models offers a practical alternative, delivering high-quality solutions.

Therefore, the choice of DRTO strategy under current computational constraints largely depends on model availability. If a full-order process model is accessible and allows for tractable and robust local optimization, high-fidelity models with local optimization methods are preferable. Conversely, if only plant data or simplified mechanistic models are available, nonlinear SBMs become more suitable. Given the high computational cost of globally solving nonconvex scheduling problems, a combination of search space exploration and local optimization (e.g., through multistart) is often sufficient.

Lastly, we point out that our conclusions stem from a specific industrial process and the consideration of a single electricity price profile. Thanks to the highly nonlinear dynamics entailed, the feature of both path and terminal operational constraints for scheduling and the consideration of a representative price profile with average fluctuating behavior,[77] our case study is expected to provide a character-

https://doi.org/10.1021/acs.iecr.5c02705
Ind. Eng. Chem. Res. 2025, 64, 21641−21657

istic example. However, future work should focus on a comparative analysis of a variety of applications for more generalizable results incorporating further SBM options,[32] optimization techniques (e.g., learning-based methods[52]), and operational scenarios. The latter would incorporate elaborate scheduling considerations such as sequencing, inventory, market, and resource constraints, among others.[19,88] Such setups capture realistic scenarios, while also increasing computational complexity by introducing additional integer and intertemporal decisions, along with a large number of variables. Additionally, improvements in the scaling behavior of global dynamic optimization should be investigated regarding constructing tighter relaxations for the lower bounding problem,[89] the ODE system[90] or the neural networks.[91] Future advancements in parallel computing and quantum optimization are expected to significantly enhance tractability of global optimization problems.

■ ASSOCIATED CONTENT

Supporting Information

The Supporting Information is available free of charge at https://pubs.acs.org/doi/10.1021/acs.iecr.5c02705.

Production set points and output of training and validation for the scale-bridging models provided (CSV)

Data-driven model hyperparameters, identification metrics, and parameter values. DRTO and tNMPC variable bounds, initialization, constraints and numerical results. Electricity price profiles. Process-model mismatch and relaxation effect on optimization results (PDF)

■ AUTHOR INFORMATION

Corresponding Author

Alexander Mitsos − *JARA-ENERGY, 52056 Aachen, Germany; Process Systems Engineering (AVT.SVT), RWTH Aachen University, 52074 Aachen, Germany; Energy Systems Engineering (ICE-1), Forschungszentrum Jülich, 52425 Jülich, Germany;* orcid.org/0000-0003-0335-6566; Email: amitsos@alum.mit.edu

Authors

Chrysanthi Papadimitriou − *Process Systems Engineering (AVT.SVT), RWTH Aachen University, 52074 Aachen, Germany;* orcid.org/0009-0009-1865-1016

Michael Baldea − *McKetta Department of Chemical Engineering, The University of Texas at Austin, Austin, Texas 78712, United States; Oden Institute for Computational Engineering and Sciences, The University of Texas at Austin, Austin, Texas 78712, United States;* orcid.org/0000-0001-6400-0315

Complete contact information is available at: https://pubs.acs.org/10.1021/acs.iecr.5c02705

Author Contributions

C.P.: Conceptualization, Methodology, Investigation, Software, Validation, Formal analysis, Writing—Original Draft, Visualization. M.B.: Supervision (supporting), Validation, Writing—Review & Editing. A.M.: Supervision (lead), Validation, Writing—Review & Editing, Resources, Project administration, Funding acquisition.

Notes

The authors declare no competing financial interest.

■ ACKNOWLEDGMENTS

The authors gratefully acknowledge the financial support of and the Deutsche Forschungsgemeinschaft (DFG, German Research Foundation)333849990/GRK2379 (IRTG Hierarchical and Hybrid Approaches in Modern Inverse Problems). Simulations were performed with computing resources granted by RWTH Aachen University under project rwth1797. Moreover, we thank Clara Witte, Jan Christoph Schulze and Susanne Sass for valuable discussions and advice throughout the development of this work.

■ LIST OF ACRONYMS

DRTO	dynamic real-time optimization
MILP	mixed-integer linear program
(MI)LP	(mixed-integer) linear program
NLP	nonlinear program
LP	linear program
SBM	scale-bridging model
B&B	branch-and-bound
HW	Hammerstein-Wiener
SISO	single-input-single-output
IDS	integrated dynamic scheduling
MPC	model predictive control
tNMPC	tracking nonlinear model predictive control
FSR	finite-step response
ARX	autoregressive with extra inputs
ASU	air separation unit
MVs	manipulated variables
CVs	controlled variables
SRVs	scheduling-relevant variables
SI	supporting information
SOS2	special ordered sets of the second type
PWL	piecewise linear
ANNs	artificial neural networks
DoFs	degrees of freedom
NRMSE	normalized root mean squared error
DA	day-ahead
LSS	linear state-space
DyOS	dynamic optimization software
FMU	functional mockup unit
SS	steady-state

■ NOMENCLATURE

Integer

r	binary variable for SOS2 reformulation
j	piecewise linear function breakpoint

Continuous variables

t	time
h	input to Wiener block
P	total power consumption (MW)
C^{e}	electricity price (€/MWh)
$\overline{z}$	full-order mechanistic process model M2 states
$\overline{y}$	full-order mechanistic process model M2 outputs
F_{asu}	ASU production rate (mol/s)
$F_{tank,in}$	storage tank input rate (mol/s)
$F_{tank,out}$	storage tank output rate (mol/s)
F_{drain}	reboiler liquid drain (mol/s)
F_{dem}	product demand (mol/s)
$\boldsymbol{x}$	tNMPC states
N_{tank}	tank hold-up (kmol)
N_{irc}	IRC hold-up (kmol)
ΔT_{irc}	IRC temperature difference (K)

ξ_{liq} split fraction of product to liquefier (−)
ξ_{top} column reflux ration (−)
ξ_{turb} split fraction of air to turbine (−)
P_{asu} ASU energy consumption (kW)
P_{liq} energy consumption of liquefier (kW)
P_{mac} energy consumption of compressor (kW)
P_{turb1} energy production of first turbine (kW)
$\boldsymbol{x}_{p,sp}$ tNMPC set points
$\boldsymbol{x}_{p}$ tNMPC controlled variables CVs
P_{turb2} energy production of second turbine (kW)
I_{asu} ASU product impurity level (ppm)
P_{liq} energy consumption of liquefier (kW)
w output to Hammerstein block
λ SOS2 variable
t' time
bp piecewise linear breakpoint position
pw piecewise linear breakpoint value
$\boldsymbol{x}_{1,sp}$ constant tNMPC set points
$\boldsymbol{x}_{0}$ initial tNMPC state condition
$\boldsymbol{u}$ tNMPC controls, manipulated variables MVs
$\boldsymbol{v}_{sched,sp}$, $\boldsymbol{v}$ time-varying set points of scheduling-relevant variables SRVs/SBM inputs
$\boldsymbol{z}$ SBM states
$\boldsymbol{y}$ SBM outputs

Functions

f full-order mechanistic process model M2
f_{liq} liquefier energy consumption model
f^{SBM} scale-bridging model
f_{H} Hammerstein function
f_{W} Wiener function
$A(q)$ ARX n_a-degree polynomial
$B(q)$ ARX n_b-degree polynomial
$f^{Mechanistic}$ full-order mechanistic process model M2
$\boldsymbol{c}$ scheduling constraints

Indices

t control discretization interval
s state discretization interval
i' state discretization interval
i scale-bridging model indicator

Indicators

$_{sp}$ set point
$_{0}$ initial condition
^{min} lower bound
^{max} upper bound
$\hat{}$ discretized variable
$_{1}$ ASU production rate scale-bridging model
$_{2}$ ASU energy consumption scale-bridging model
$_{H}$ Hammerstein block
$_{W}$ Wiener block

Parameters

t_0 starting time point of tNMPC
n_a ARX polynomial degree of denominator
n_b ARX polynomial degree of nominator
$\boldsymbol{e}$ ARX white noise vector
ω_i weights in tNMPC objective
α polytropic head of liquefier
a ARX coefficient of polynomial $A(q)$
b ARX coefficient of polynomial $B(q)$
l number of states
τ_s scheduling horizon length
n_d ARX delay parameter
τ_c control/prediction horizon length
Δt_u control discretization step
Δt_s state discretization step
$\boldsymbol{A,b,c}$, $\boldsymbol{D}$ linear state-space model matrices
$\boldsymbol{A,b,c}$, d single-input-single-output linear state-space model matrices
S_s FSR step response coefficient
n number of control intervals
k number of state intervals within a single control interval

Sets

$\mathcal{T}_c$ control/prediction horizon
$\mathcal{T}_s$ scheduling horizon

REFERENCES

(1) Floudas, C. A.; Lin, X. Mixed integer linear programming in process scheduling: Modeling, algorithms, and applications. *Ann. Oper. Res.* **2005**, *139*, 131−162.
(2) Paulus, M.; Borggrefe, F. The potential of demand-side management in energy-intensive industries for electricity markets in Germany. *Applied Energy* **2011**, *88*, 432−441.
(3) Mitsos, A.; Asprion, N.; Floudas, C. A.; Bortz, M.; Baldea, M.; Bonvin, D.; Caspari, A.; Schäfer, P. Challenges in process optimization for new feedstocks and energy sources. *Comput. Chem. Eng.* **2018**, *113*, 209−221.
(4) Bhatia, T.; Biegler, L. T. Dynamic Optimization in the Design and Scheduling of Multiproduct Batch Plants. *Ind. Eng. Chem. Res.* **1996**, *35*, 2234−2246.
(5) Flores-Tlacuahuac, A.; Grossmann, I. E. Simultaneous cyclic scheduling and control of a multiproduct CSTR. *Ind. Eng. Chem. Res.* **2006**, *45*, 6698−6712.
(6) Baldea, M.; Harjunkoski, I. Integrated production scheduling and process control: A systematic review. *Comput. Chem. Eng.* **2014**, *71*, 377−390.
(7) Seborg, D. E.; Edgar, T. F.; Mellichamp, D. A.; Doyle, F. J., III *Process Dynamics and Control*; John Wiley & Sons, 2016.
(8) Tosukhowong, T.; Lee, J. M.; Lee, J. H.; Lu, J. An introduction to a dynamic plant-wide optimization strategy for an integrated plant. *Comput. Chem. Eng.* **2004**, *29*, 199−208.
(9) Engell, S. Feedback control for optimal process operation. *J. Process Control* **2007**, *17*, 203−219.
(10) Amrit, R.; Rawlings, J. B.; Biegler, L. T. Optimizing process economics online using model predictive control. *Comput. Chem. Eng.* **2013**, *58*, 334−343.
(11) Ellis, M.; Durand, H.; Christofides, P. D. A tutorial review of economic model predictive control methods. *J. Process Control* **2014**, *24*, 1156−1178.
(12) Caspari, A.; Tsay, C.; Mhamdi, A.; Baldea, M.; Mitsos, A. The integration of scheduling and control: Top-down vs. bottom-up. *J. Process Control* **2020**, *91*, 50−62.
(13) Helbig, A.; Abel, O.; Marquardt, W. *Nonlinear Model Predictive Control* **2000**, 295−311.
(14) Chatzidoukas, C.; Kiparissides, C.; Perkins, J. D.; Pistikopoulos, E. N. *Process Systems Engineering 2003, 8th International Symposium on Process Systems Engineering*; Comput.-Aided Chem. Eng.2003; Vol. 15, pp 744−747.
(15) Mahadevan, R.; Doyle, F. J.; Allcock, A. C. Control-relevant scheduling of polymer grade transitions. *AIChE J.* **2002**, *48*, 1754−1764.
(16) Chu, Y.; You, F. Integration of scheduling and control with online closed-loop implementation: Fast computational strategy and large-scale global optimization algorithm. *Comput. Chem. Eng.* **2012**, *47*, 248−268.
(17) Jamaludin, M. Z.; Swartz, C. L. Closed-loop Formulation for Nonlinear Dynamic Real-time Optimization. *IFAC-PapersOnLine* **2016**, *49*, 406−411.

https://doi.org/10.1021/acs.iecr.5c02705
Ind. Eng. Chem. Res. 2025, 64, 21641−21657

(18) Simkoff, J. M.; Baldea, M. Production scheduling and linear MPC: Complete integration via complementarity conditions. *Comput. Chem. Eng.* **2019**, *125*, 287−305.
(19) Méndez, C. A.; Cerdá, J.; Grossmann, I. E.; Harjunkoski, I.; Fahl, M. State-of-the-art review of optimization methods for short-term scheduling of batch processes. *Comput. Chem. Eng.* **2006**, *30*, 913−946.
(20) Nwadinobi, C.; Ezeaku, I. Review of maintenance scheduling and optimization models. *Int. J. Scientific Res. Mech. Mater. Eng.* **2018**, *2*, 23−35.
(21) Fei, H.; Li, Q.; Sun, D. A Survey of Recent Research on Optimization Models and Algorithms for Operations Management from the Process View. *Sci. Program.* **2017**, *2017*, No. 7219656.
(22) Yu, S.; You, L.; Zhou, S. A review of optimization modeling and solution methods in renewable energy systems. *Front. Eng. Management* **2023**, *10*, 640−671.
(23) Tseremoglou, I.; van Kessel, P. J.; Santos, B. F. A Comparative Study of Optimization Models for Condition-Based Maintenance Scheduling of an Aircraft Fleet. *Aerospace* **2023**, *10*, 120.
(24) Kelley, M. T.; Pattison, R. C.; Baldick, R.; Baldea, M. An MILP framework for optimizing demand response operation of air separation units. *Appl. Energy* **2018**, *222*, 951−966.
(25) Kelley, M. T.; Pattison, R. C.; Baldick, R.; Baldea, M. An efficient MILP framework for integrating nonlinear process dynamics and control in optimal production scheduling calculations. *Comput. Chem. Eng.* **2018**, *110*, 35−52.
(26) Kelley, M. T.; Tsay, C.; Cao, Y.; Wang, Y.; Flores-Cerrillo, J.; Baldea, M. A data-driven linear formulation of the optimal demand response scheduling problem for an industrial air separation unit. *Chem. Eng. Sci.* **2022**, *252*, No. 117468.
(27) Dias, L. S.; Ierapetritou, M. G. 110th anniversary: Integration of scheduling and robust model predictive control. *Ind. Eng. Chem. Res.* **2020**, *59*, 265−280.
(28) Tsay, C.; Baldea, M. Integrating production scheduling and process control using latent variable dynamic models. *Control Eng. Pract.* **2020**, *94*, No. 104201.
(29) Rodríguez Vera, H. U.; Ricardez-Sandoval, L. A. Integration of Scheduling and Control for Chemical Batch Plants under Stochastic Uncertainty: A Back-Off Approach. *Ind. Eng. Chem. Res.* **2022**, *61*, 4363−4378.
(30) Schulze, J. C.; Caspari, A.; Offermanns, C.; Mhamdi, A.; Mitsos, A. Nonlinear model predictive control of ultra-high-purity air separation units using transient wave propagation model. *Comput. Chem. Eng.* **2021**, *145*, No. 107163.
(31) Pattison, R. C.; Touretzky, C. R.; Johansson, T.; Harjunkoski, I.; Baldea, M. Optimal process operations in fast-changing electricity markets: framework for scheduling with low-order dynamic models and an air separation application. *Ind. Eng. Chem. Res.* **2016**, *55*, 4562−4584.
(32) Tsay, C.; Baldea, M. 110th anniversary: Using data to bridge the time and length scales of process systems. *Ind. Eng. Chem. Res.* **2019**, *58*, 16696−16708.
(33) Đukić, S.; Sarić, A. Dynamic model reduction: An overview of available techniques with application to power systems. *Serbian J. Electrical Eng.* **2012**, *9*, 131−169.
(34) Cao, Y.; Swartz, C. L. E.; Flores-Cerrillo, J. Optimal dynamic operation of a high-purity air separation plant under varying market conditions. *Ind. Eng. Chem. Res.* **2016**, *55*, 9956−9970.
(35) Schäfer, P.; Caspari, A.; Kleinhans, K.; Mhamdi, A.; Mitsos, A. Reduced dynamic modeling approach for rectification columns based on compartmentalization and artificial neural networks. *AIChE J.* **2019**, *65*, No. e16568.
(36) Kumar, P.; Rawlings, J. B.; Wright, S. J. Industrial, large-scale model predictive control with structured neural networks. *Comput. Chem. Eng.* **2021**, *150*, No. 107291.
(37) Dering, D.; Swartz, C. L. Integration of Scheduling and Control for Plants Controlled by Distributed MPC Systems. *Ind. Eng. Chem. Res.* **2024**, *63*, 12016−12034.
(38) Baader, F. J.; Althaus, P.; Bardow, A.; Dahmen, M. Dynamic ramping for demand response of processes and energy systems based on exact linearization. *J. Process Control* **2022**, *118*, 218−230.
(39) Du, J.; Park, J.; Harjunkoski, I.; Baldea, M. A time scale-bridging approach for integrating production scheduling and process control. *Comput. Chem. Eng.* **2015**, *79*, 59−69.
(40) Lucia, D. J.; Beran, P. S.; Silva, W. A. Reduced-order modeling: new approaches for computational physics. *Prog. Aeronaut. Sci.* **2004**, *40*, 51−117.
(41) Burnak, B.; Katz, J.; Diangelakis, N. A.; Pistikopoulos, E. N. Simultaneous Process Scheduling and Control: A Multiparametric Programming-Based Approach. *Ind. Eng. Chem. Res.* **2018**, *57*, 3963−3976.
(42) Schulze, J. C.; Doncevic, D. T.; Erwes, N.; Mitsos, A. *FOCAPO/CPC Proc.* San Diego, CA, USA 2023.
(43) Caspari, A.; Faust, J. M. M.; Schäfer, P.; Mhamdi, A.; Mitsos, A. Economic nonlinear model predictive control for flexible operation of air separation units. *IFAC-PapersOnLine* **2018**, *51*, 295−300.
(44) Simkoff, J. M.; Baldea, M. Stochastic Scheduling and Control Using Data-Driven Nonlinear Dynamic Models: Application to Demand Response Operation of a Chlor-Alkali Plant. *Ind. Eng. Chem. Res.* **2020**, *59*, 10031−10042.
(45) Schulze, J. C.; Mitsos, A. Nonlinear Model Order Reduction of Dynamical Systems in Process Engineering: Review and Comparison, 2025, arXiv:2506.12819. arXiv.org e-Print archive https://arxiv.org/abs/2506.12819.
(46) Biegler, L. T. Nonlinear programming strategies for dynamic chemical process optimization. *Theor. Found. Chem. Eng.* **2014**, *48*, 541−554.
(47) Papadimitriou, C.; Varelmann, T.; Schröder, C.; Jupke, A.; Mitsos, A. Globally optimal scheduling of an electrochemical process via data-driven dynamic modeling and wavelet-based adaptive grid refinement. *Optimization Eng.* **2023**, *25*, 1719−1757.
(48) Mendez, C. A.; Cerdá, J. An MILP framework for batch reactive scheduling with limited discrete resources. *Comput. Chem. Eng.* **2004**, *28*, 1059−1068.
(49) Harjunkoski, I.; Grossmann, I. E. Decomposition techniques for multistage scheduling problems using mixed-integer and constraint programming methods. *Comput. Chem. Eng.* **2002**, *26*, 1533−1552.
(50) Maravelias, C. T.; Grossmann, I. E. A hybrid MILP/CP decomposition approach for the continuous time scheduling of multipurpose batch plants. *Comput. Chem. Eng.* **2004**, *28*, 1921−1949.
(51) Vassiliadis, V. S.; Sargent, R. W.; Pantelides, C. C. Solution of a class of multistage dynamic optimization problems. 2. Problems with path constraints. *Ind. Eng. Chem. Res.* **1994**, *33*, 2123−2133.
(52) Zhang, C.; Juraschek, M.; Herrmann, C. Deep reinforcement learning-based dynamic scheduling for resilient and sustainable manufacturing: A systematic review. *J. Manuf. Syst.* **2024**, *77*, 962−989.
(53) Baykasoğlu, A.; Ozsoydan, F. B. Dynamic scheduling of parallel heat treatment furnaces: A case study at a manufacturing system. *J. Manuf Syst.* **2018**, *46*, 152−162.
(54) Sass, S.; Faulwasser, T.; Hollermann, D. E.; Kappatou, C. D.; Sauer, D.; Schütz, T.; Shu, D. Y.; Bardow, A.; Gröll, L.; Hagenmeyer, V.; Müller, D.; Mitsos, A. Model compendium, data, and optimization benchmarks for sector-coupled energy systems. *Comput. Chem. Eng.* **2020**, *135*, No. 106760.
(55) Biegler, L. T.; Zavala, V. M. Large-scale nonlinear programming using IPOPT: An integrating framework for enterprise-wide dynamic optimization. *Comput. Chem. Eng.* **2009**, *33*, 575−582.
(56) Terrazas-Moreno, S.; Flores-Tlacuahuac, A.; Grossmann, I. E. Simultaneous cyclic scheduling and optimal control of polymerization reactors. *AIChE J.* **2007**, *53*, 2301−2315.
(57) Biegler, L. T. Integrated optimization strategies for dynamic process operations. *Theor. Found. Chem. Eng.* **2017**, *51*, 910−927.
(58) Shi, H.; You, F. A novel adaptive surrogate modeling-based algorithm for simultaneous optimization of sequential batch process scheduling and dynamic operations. *AIChE J.* **2015**, *61*, 4191−4209.

https://doi.org/10.1021/acs.iecr.5c02705
Ind. Eng. Chem. Res. 2025, 64, 21641−21657

(59) Capón-García, E.; Guillén-Gosálbez, G.; Espuña, A. Integrating process dynamics within batch process scheduling via mixed-integer dynamic optimization. *Chem. Eng. Sci.* **2013**, *102*, 139−150.
(60) Nie, Y.; Biegler, L. T. Integrated dynamic optimization and scheduling of polymerization processes with first principle models. *Chem. Ing. Technol.* **2017**, *89*, 1490−1502.
(61) Prata, A.; Oldenburg, J.; Kroll, A.; Marquardt, W. Integrated scheduling and dynamic optimization of grade transitions for a continuous polymerization reactor. *Comput. Chem. Eng.* **2008**, *32*, 463−476.
(62) Schulze, J. C.; Papadimitriou, C.; Kolmer, P.; Mitsos, A. An Integrated Scheduling and Control Scheme with Two Economic Layers for Demand Side Management of Chemical Processes. *AIChE J.* **2025**, *71*, No. e18731.
(63) Nie, Y.; Biegler, L. T.; Villa, C. M.; Wassick, J. M. Discrete Time Formulation for the Integration of Scheduling and Dynamic Optimization. *Ind. Eng. Chem. Res.* **2015**, *54*, 4303−4315.
(64) Liu, J.; Qiao, F.; Zou, M.; Zinn, J.; Ma, Y.; Vogel-Heuser, B. Dynamic scheduling for semiconductor manufacturing systems with uncertainties using convolutional neural networks and reinforcement learning. *Complex Intell. Syst.* **2022**, *8*, 4641−4662.
(65) Mitrai, I.; Daoutidis, P. *AIChE Annual Meeting, Conf. Proc.*, 2024.
(66) Kappatou, C. D.; Bongartz, D.; Najman, J.; Sass, S.; Mitsos, A. Global dynamic optimization with Hammerstein-Wiener models embedded. *J. Glob. Optim.* **2022**, *84*, 321−347.
(67) Singer, A. B.; Barton, P. I. Global solution of optimization problems with parameter-embedded linear dynamic systems. *J. Optimization Theory Applications* **2004**, *121*, 613−646.
(68) Singer, A. B.; Barton, P. I. Global optimization with nonlinear ordinary differential equations. *J. Glob. Optim.* **2006**, *34*, 159−190.
(69) Wise, B. M.; Ricker, N. Identification of finite impulse response models with continuum regression. *J. Chemom.* **1993**, *7*, 1−14.
(70) Dayal, B. S.; MacGregor, J. F. Identification of finite impulse response models: methods and robustness issues. *Ind. Eng. Chem. Res.* **1996**, *35*, 4078−4090.
(71) Kadam, J.; Marquardt, W.; Schlegel, M.; Backx, T.; Bosgra, O.; Brouwer, P. J.; Dünnebier, G.; van Hessem, D.; Tiagounov, A.; de Wolf, S. Towards integrated dynamic real-time optimization and control of industrial processes. *FOCAPO Proceedings* **2003**, 593−596.
(72) Zhuge, J.; Ierapetritou, M. G. Integration of scheduling and control with closed loop implementation. *Ind. Eng. Chem. Res.* **2012**, *51*, 8550−8565.
(73) Swartz, C. L. E.; Kawajiri, Y. Design for dynamic operation-A review and new perspectives for an increasingly dynamic plant operating environment. *Comput. Chem. Eng.* **2019**, *128*, 329−339.
(74) Nyström, R. H.; Franke, R.; Harjunkoski, I.; Kroll, A. Production campaign planning including grade transition sequencing and dynamic optimization. *Comput. Chem. Eng.* **2005**, *29*, 2163−2179.
(75) Rawlings, J. B.; Mayne, D. Q.; Diehl, M. *Model Predictive Control: Theory, Computation, and Design*, 2nd ed.; Nob Hill Publishing, 2017.
(76) Kelley, M. T. Dynamic Modeling and Optimal Scheduling of Chemical Processes Participating in Fast-Changing Electricity Markets: A Data-Driven Approach. Ph.D. Thesis, University of Texas at Austin2021.
(77) Papadimitriou, C.; Schulze, J. C.; Mitsos, A. A Practical Scenario Generation Method for Electricity Prices on Day-Ahead and Intraday Spot Markets. *Comput. Chem. Eng.* **2025**, *199*, No. 109118.
(78) Caspari, A.; Offermanns, C.; Schäfer, P.; Mhamdi, A.; Mitsos, A. A flexible air separation process: 1. Design and steady-state optimizations. *AIChE J.* **2019**, *65*, No. e16705.
(79) Hannemann, R.; Marquardt, W.; Naumann, U.; Gendler, B. Discrete first-and second-order adjoints and automatic differentiation for the sensitivity analysis of dynamic models. *Procedia Comput. Sci.* **2010**, *1*, 297−305.
(80) Gill, P. E.; Murray, W.; Saunders, M. A. SNOPT: An SQP algorithm for large-scale constrained optimization. *SIAM Rev.* **2005**, *47*, 99−131.
(81) Bongartz, D.; Najman, J.; Sass, S.; Mitsos, A. *MAiNGO - McCormick-based Algorithm for mixed-integer Nonlinear Global Optimization; Process Systems Engineering (AVT.SVT)*; RWTH Aachen University, 2018.
(82) McCormick, G. P. Computability of global solutions to factorable nonconvex programs: Part I - Convex underestimating problems. *Math. Program.* **1976**, *10*, 147−175.
(83) Mitsos, A.; Chachuat, B.; Barton, P. I. McCormick-based relaxations of algorithms. *SIAM J. Optimization* **2009**, *20*, 573−601.
(84) Tsoukalas, A.; Mitsos, A. Multivariate McCormick relaxations. *J. Glob. Optim.* **2014**, *59*, 633−662.
(85) Wächter, A.; Biegler, L. T. On the implementation of an interior-point filter line-search algorithm for large-scale nonlinear programming. *Math. Program.* **2006**, *106*, 25−57.
(86) Schweidtmann, A. M.; Mitsos, A. Deterministic global optimization with artificial neural networks embedded. *J. Optimization Theory Applications* **2019**, *180*, 925−948.
(87) Zagrobelny, M.; Ji, L.; Rawlings, J. B. Quis custodiet ipsos custodes? *Ann. Rev. Control* **2013**, *37*, 260−270.
(88) Maravelias, C. T. General framework and modeling approach classification for chemical production scheduling. *AIChE J.* **2012**, *58*, 1812−1828.
(89) Castro, P. M. Tightening piecewise McCormick relaxations for bilinear problems. *Comput. Chem. Eng.* **2015**, *72*, 300−311.
(90) Sahlodin, A. M.; Chachuat, B. Convex/concave relaxations of parametric ODEs using Taylor models. *Comput. Chem. Eng.* **2011**, *35*, 844−857.
(91) Witte, C.; Lüthje, J. T.; Schulte, V.; Mitsos, A.; Bongartz, D. Deterministic global optimization with trained neural networks: Is the envelope of single neurons worth it? *Optimization online preprint:* https://optimization-online.org/?p/30062, 2025.